Hindawi
Shock and Vibration
Volume 2018, Article ID 3129834, 16 pages
https://doi.org/10.1155/2018/3129834

Research Article

Attitude Maneuvering and Vibration Reducing Control of Flexible Spacecraft Subject to Actuator Saturation and Misalignment

Jiawei Tao,[1,2] Tao Zhang ,[2] and Yongfang Nie[3]

[1]*National Key Laboratory of Science and Technology on Space Intelligent Control, Beijing Institute of Control Engineering, Beijing, China*
[2]*Department of Automation, School of Information Science and Technology, Tsinghua University, Beijing, China*
[3]*Department of Strategic Missile and Underwater Weapon, Naval Submarine Academy, Qingdao, China*

Correspondence should be addressed to Tao Zhang; taozhang@tsinghua.edu.cn

Received 18 October 2017; Revised 17 June 2018; Accepted 5 July 2018; Published 5 September 2018

Academic Editor: Jussi Sopanen

A robust adaptive constrained control scheme is proposed for flexible spacecraft attitude maneuver and vibration suppression, in which multiple constraints are simultaneously considered, such as uncertain inertia parameters, external disturbance, unmeasured elastic vibration, actuator saturation, and even actuator misalignment. More specifically, a novel path planning scheme based on quintic polynomial transition is firstly developed to realize smooth acceleration variate and therefore decrease the vibration of flexible appendages. Secondly, an elastic modal estimator is employed to estimate the unmeasured variables, such as the modal position and velocity. Thirdly, an adaptive updating technique is used to spare the extra knowledge of system parameters and the bound of the external disturbance. In addition, an auxiliary design system is constructed to address the actuator saturation problem, and a compensation term is synthesized and integrated into the controller to handle the actuator misalignment. Finally, overall system stabilization is proved within the framework of Lyapunov theory, and numerical simulation results are presented to illustrate the effectiveness of the proposed scheme.

1. Introduction

Flexible spacecraft with large flexible structures is usually expected to achieve high pointing and fast attitude maneuvering in future space missions. However, the attitude maneuvering operation will introduce certain levels of vibration to flexible appendages due to the rigid-flexible coupling effect, which will deteriorate its pointing performance. For flexible spacecrafts, the governing differential equations for attitude kinematics and dynamics are strongly nonlinear in nature. The attitude maneuvering problem is further complicated by the uncertainty of spacecraft inertia parameters due to onboard payload motion and fuel consumption. Furthermore, it is also affected by various external disturbances that influence the mission objectives significantly. Additionally, the actuator misalignment during installation and actuator saturation increases the complexity and difficulty further.

All these factors in a realistic environment cause a considerable difficulty in the design of attitude control system for meeting high-precision pointing requirement and desired control performance during the attitude maneuver process, especially when all these issues are treated simultaneously.

Over the last few decades, considerable works have been found for vibration suppression and attitude control system design. A nonlinear state feedback attitude control law [1] in combination with path planning is proposed. Specifically, the planned attitude maneuver path is smooth, and thus, appendages' vibration excited by attitude maneuver can be attenuated greatly. Specially, variable structure control (VSC) is known as an efficient way to deal with system uncertainty and external disturbance and has been applied to attitude control problem of flexible spacecrafts in [2, 3].

However, these design methods require the information on the bounds on the uncertainties or disturbances for the computation of control gains. Recently, to overcome the drawbacks of each method, a combination of these techniques with adaptation mechanism to tune the controller gains are also studied for flexible spacecrafts with parameter uncertainties and disturbances [4–6]. A new adaptive system [4] for rotational maneuver and vibration suppression of an orbiting spacecraft with flexible appendages has been designed. Then adaptive output regulation of the closed-loop system is accomplished in spite of parameter uncertainties and disturbances. A new variable structure control approach [5] has been proposed for attitude control and vibration suppression of flexible spacecrafts during attitude maneuvering, and the adaptive version of the proposed controller is achieved through releasing the limitation of knowing the bounds of the uncertainties and perturbations in advance.

Relevant drawback of these control strategies is either the extra necessity to measure the modal variables or to treat the rigid-flexible coupling effect as an additional disturbance acting on a rigid structure. With regard to the latter situation, an extended state observer [7, 8] is designed to estimate and thus to attenuate the total disturbance in finite time, including an external disturbance torque and the coupling effect. As a result, the prior knowledge of the total disturbance is not required.

Unfortunately, in some cases, the availability of the measured modal variables is an unrealistic hypothesis due to the impracticability of using appropriate sensors or the economical requisite. For removing this disadvantage, reconstructing the unmeasured modal position and velocity by means of appropriate dynamics is an alternative way. A class of nonlinear controllers incorporating modal state estimator [9–13] has been derived for spacecraft with flexible appendages. It does not ask for measures of the modal variables, but only uses the parameters describing the attitude and the spacecraft angular velocity. The controller derived then uses estimates of the modal variables and its rate to avoid direct measurement.

However, a typical feature in all of the mentioned attitude-control schemes and methods is that the control device is assumed to be able to produce big enough control torque without taking actuator saturation into account. Extensive results pertaining to spacecraft attitude control systems containing actuator saturation nonlinearities have been presented in [14–22]. A robust variable structure controller in [14, 15] has been skillfully designed to control the spacecraft attitude under input saturation. However, these control schemes lose the generality to nonlinear flexible spacecraft system. A modified adaptive backstepping attitude controller [17, 18] is developed considering external disturbances and input saturation. But the way to include the effects of the flexible dynamics in the lumped disturbance for the rigid dynamics deprives the controller of a direct compensation of the dynamic terms caused by the flexibility.

A typical feature in the previous approaches is that they do not consider actuator misalignments. However, whether due to finite manufacturing tolerances or warping of the spacecraft structure during launch, some actuator alignment error will definitely exist in practice. This problem may cause mission performance to degrade and thus pose significant risk to the successful operation of the spacecraft. Therefore, it is desirable to design a control scheme to handle the actuator misalignments. Unfortunately, there has been insufficient research on attitude control in the presence of actuator misalignments. An adaptive control law [23] is developed to accomplish attitude maneuver in the presence of relatively small gimbals' alignment error of variable speed control moment gyros.

More specially, an adaptive control approach [24] was proposed for satellite formation flying. The backstepping technique is used to synthesize the controller, and the thrust misalignment is successfully handled. In another related work, a nonlinear model reference adaptive control scheme [25] is tested in the presence of misalignment errors up to fifteen degrees. Although an extended Kalman filter is used in another approach to develop methods for on-orbit actuator alignment calibration, uncertain inertia properties have not been taken into account.

With a view to handle the above challenges and potential problems simultaneously, a new constrained robust adaptive control scheme is proposed in this paper. The main contributions are summarized as follows:

(1) A novel path planning scheme based on quantic polynomial transition is applied to smooth acceleration variate and therefore decrease the vibration of flexible appendages.

(2) This paper investigates the feasibility of attitude maneuver and vibration suppression in the presence of uncertain inertia parameters, external disturbances, unmeasured elastic vibrations, actuator saturation, and even actuator misalignment simultaneously, which has not been previously examined. As compared with the controller in [16] which only considers attitude stabilization, that is, rest-to-rest maneuver of a flexible spacecraft, the control scheme in the present paper can be applied to handle attitude tracking control problem. The controller in [6] investigates the attitude tracking problem for flexible spacecrafts, while it does not take the actuator saturation and actuator misalignment into consideration explicitly.

(3) The proposed controller is designed without requiring prior knowledge of the measurement of vibration variables, of the parameter uncertainties, and the upper bound of external disturbance. Robust control terms are synthesized to compensate all uncertainties including parametric uncertainties, unmeasured elastic vibration, external disturbances, actuator saturation, and actuator misalignment.

The rest of this paper is organized as follows: Section 2 states flexible spacecraft modelling with actuator misalignment and control problem formulation. A constrained robust adaptive-control scheme is proposed in Section 3. Numerical simulation results are presented in Section 4 to demonstrate the effectiveness and superiority of the proposed control scheme. Finally, conclusion is given in Section 5.

2. Flexible Spacecraft Modelling and Problem Formulation

2.1. Kinematics and Dynamics Equation. This section briefly reviews the quaternion mathematical description of the attitude motion of a flexible spacecraft.

The attitude kinematic equation of the spacecraft can be written in terms of unit quaternion for global representation without singularities as follows [26]:

$$\dot{\mathbf{q}} = \begin{bmatrix} \dot{q}_0 \\ \dot{\mathbf{q}}_v \end{bmatrix} = \frac{1}{2} \begin{bmatrix} -\mathbf{q}_v^T \\ q_0 \mathbf{I}_3 + \mathbf{q}_v^{\times} \end{bmatrix} \boldsymbol{\omega}, \tag{1}$$

where $\mathbf{q} = [q_0, \ \mathbf{q}_v^T]^T$ represents the attitude quaternion, and $\mathbf{I}$ is an identity matrix of the dimension specified by its subscript.

The dynamic model of a flexible spacecraft is governed by the following differential equations:

$$\mathbf{J}\dot{\boldsymbol{\omega}} + \boldsymbol{\delta}^T \ddot{\boldsymbol{\eta}} = -\boldsymbol{\omega}^{\times}\left(\mathbf{J}\boldsymbol{\omega} + \boldsymbol{\delta}^T \dot{\boldsymbol{\eta}}\right) + \mathbf{u} + \mathbf{d}, \tag{2}$$

$$\ddot{\boldsymbol{\eta}} + \mathbf{C}\dot{\boldsymbol{\eta}} + \mathbf{K}\boldsymbol{\eta} = -\boldsymbol{\delta}\dot{\boldsymbol{\omega}}, \tag{3}$$

where $\boldsymbol{\omega}$ is the spacecraft angular velocity in the body-fixed frame, $\boldsymbol{\omega}^{\times}$ is the skew-symmetric matrix of $\boldsymbol{\omega}$, $\boldsymbol{\eta}$ is the modal coordinate vector of the flexible appendages, the matrix $\mathbf{J}$ denotes the total inertia of spacecraft moment, $\boldsymbol{\delta}$ is the coupling matrix between the flexible appendages and the rigid spacecraft, $\mathbf{u}$ is the control torque, $\mathbf{d}$ is the external disturbance torque vector, and $\mathbf{C}$ and $\mathbf{K}$ denote the damping and stiffness matrices, respectively, and they are defined as

$$\begin{aligned} \mathbf{C} &= \operatorname{diag}\{2\xi_i \omega_{ni}, \ i = 1, \ \ldots, \ N\}, \\ \mathbf{K} &= \operatorname{diag}\{\omega_{ni}^2, \ i = 1, \ \ldots, \ N\}, \end{aligned} \tag{4}$$

where N is the number of elastic modes considered, ω_{ni} is the natural frequency, and ξ_i is the corresponding damping ratio.

For simplicity of the development, let us first introduce the following variable $\boldsymbol{\psi} = \dot{\boldsymbol{\eta}} + \boldsymbol{\delta}\boldsymbol{\omega}$ representing the total angular velocity expressed in modal variables, so the dynamics of the flexible spacecraft from (2) to (3) can be further expressed as

$$\begin{bmatrix} \dot{\boldsymbol{\eta}} \\ \dot{\boldsymbol{\psi}} \end{bmatrix} = \begin{bmatrix} \mathbf{0} & \mathbf{I} \\ -\mathbf{K} & -\mathbf{C} \end{bmatrix} \begin{bmatrix} \boldsymbol{\eta} \\ \boldsymbol{\psi} \end{bmatrix} + \begin{bmatrix} -\mathbf{I} \\ \mathbf{C} \end{bmatrix} \boldsymbol{\delta}\boldsymbol{\omega}, \tag{5}$$

$$\mathbf{J}_m \dot{\boldsymbol{\omega}} = -\boldsymbol{\omega}^{\times}\left(\mathbf{J}_{mb}\boldsymbol{\omega} + \boldsymbol{\delta}^T \boldsymbol{\psi}\right) + \boldsymbol{\delta}^T \left(\mathbf{C}\boldsymbol{\psi} + \mathbf{K}\boldsymbol{\eta} - \mathbf{C}\boldsymbol{\delta}\boldsymbol{\omega}\right) + \mathbf{u} + \mathbf{d}, \tag{6}$$

where $\mathbf{J}_m = \mathbf{J} - \boldsymbol{\delta}^T \boldsymbol{\delta}$, with $\boldsymbol{\delta}^T \boldsymbol{\delta}$ as the contribution of the flexible parts to the total inertia matrix.

2.2. Attitude Tracking Model. Let $\mathbf{q}_d = [q_{d0}, \ \mathbf{q}_{dv}^T]^T$ be the unit quaternion representing the desired attitude, $\boldsymbol{\omega}_d$ be the desired angular velocity.

Then, the quaternion error $\mathbf{q}_e$ and angular velocity error $\boldsymbol{\omega}_e$ are given by

$$\mathbf{q}_e = \mathbf{q}_d^{-1} \circ \mathbf{q} = \begin{bmatrix} q_0 q_{d0} + \mathbf{q}_v^T \mathbf{q}_{dv} \\ q_{d0}\mathbf{q}_v - q_0 \mathbf{q}_{dv} + S(\mathbf{q}_v)\mathbf{q}_{dv} \end{bmatrix}, \tag{7}$$

$$\boldsymbol{\omega}_e = \boldsymbol{\omega} - \boldsymbol{\omega}_r, \tag{8}$$

where $\mathbf{q}_d^{-1}$ is the inverse of the desired attitude unit quaternion, the symbol $\circ$ is the operator for quaternion multiplication; with $\boldsymbol{\omega}_r = \mathbf{R}(\mathbf{q}_e)\boldsymbol{\omega}_d$, we have

$$\dot{\boldsymbol{\omega}}_r = -\boldsymbol{\omega}_e^{\times}\mathbf{R}(\mathbf{q}_e)\boldsymbol{\omega}_d + \mathbf{R}(\mathbf{q}_e)\dot{\boldsymbol{\omega}}_d, \tag{9}$$

where $\mathbf{R}(\mathbf{q}_e)$ is the transformation matrix from the desired coordinate frame to the body coordinate frame with

$$\mathbf{R}(\mathbf{q}_e) = \left(q_{e0}^2 - \mathbf{q}_{ev}^T \mathbf{q}_{ev}\right)\mathbf{I}_3 + 2\mathbf{q}_{ev}\mathbf{q}_{ev}^T - 2q_{e0}S(\mathbf{q}_{ev}). \tag{10}$$

From (1) to (10), tracking error dynamic equation can be obtained as follows:

$$\dot{\mathbf{q}}_e = \begin{bmatrix} \dot{q}_{e0} \\ \dot{\mathbf{q}}_{ev} \end{bmatrix} = \frac{1}{2} \begin{bmatrix} -\mathbf{q}_{ev}^T \\ q_{e0}\mathbf{I} + \mathbf{q}_{ev}^{\times} \end{bmatrix} \boldsymbol{\omega}_e, \tag{11}$$

$$\begin{aligned} \mathbf{J}_m \dot{\boldsymbol{\omega}}_e = {} & -\boldsymbol{\omega}^{\times}\mathbf{J}_m\boldsymbol{\omega} - \mathbf{J}_m\dot{\boldsymbol{\omega}}_r + \boldsymbol{\delta}^T\mathbf{K}\boldsymbol{\eta} + \boldsymbol{\delta}^T\mathbf{C}\boldsymbol{\psi} \\ & - \boldsymbol{\omega}^{\times}\boldsymbol{\delta}^T\boldsymbol{\delta}\boldsymbol{\omega} - \boldsymbol{\delta}^T\mathbf{C}\boldsymbol{\delta}\boldsymbol{\omega}_e + \mathbf{u} + \mathbf{d}, \end{aligned} \tag{12}$$

$$\begin{bmatrix} \dot{\boldsymbol{\eta}} \\ \dot{\boldsymbol{\psi}} \end{bmatrix} = \mathbf{A} \begin{bmatrix} \boldsymbol{\eta} \\ \boldsymbol{\psi} \end{bmatrix} - \mathbf{A}\mathbf{B}\boldsymbol{\delta}\boldsymbol{\omega}_e - \mathbf{B}\boldsymbol{\delta}\dot{\boldsymbol{\omega}}_r, \tag{13}$$

where $\mathbf{A}$ and $\mathbf{B}$ are given by

$$\begin{aligned} \mathbf{A} &= \begin{bmatrix} \mathbf{0} & \mathbf{I} \\ -\mathbf{K} & -\mathbf{C} \end{bmatrix}, \\ \mathbf{B} &= \begin{bmatrix} \mathbf{0} \\ \mathbf{I} \end{bmatrix}. \end{aligned} \tag{14}$$

2.3. Actuator Uncertainty Model. In practical aerospace engineering, redundant actuators are fixed to improve the reliability of the attitude control system. The considered spacecraft is controlled by using four reaction wheels. The configuration structure of four actuators in [27, 28] is adopted. Three reaction wheels are fixed orthogonally aligned with the axes of the body-fixed frame. The fourth, redundant, actuator is mounted skewed at α_4 and β_4.

With this configuration, the total control torque $\mathbf{u}$ can be calculated as

$$\mathbf{u} = \mathbf{D}\boldsymbol{\tau}, \tag{15}$$

where $\boldsymbol{\tau} = [\tau_1, \ \tau_2, \ \tau_3, \ \tau_4]^T$ denotes the nominal torque generated by the four reaction wheels, and $\mathbf{D}$ is the reaction wheel configuration matrix, representing the influence of each wheel on the angular acceleration of the spacecraft.

However, in practice, the knowledge of orthogonal configuration of actuator will never be perfect. Due to finite-manufacturing tolerances or warping of the spacecraft structure during launch, actuator misalignments may exist.

The reaction wheel mounted on the X-axis is offset from the nominal direction by constant angles, $\Delta\alpha_1$ and $\Delta\beta_1$. The reaction wheels mounted on Y-axis and Z-axis are assumed to be tilted away from their nominal directions by $\Delta\alpha_2$, $\Delta\beta_2$, $\Delta\alpha_3$, and $\Delta\beta_3$, while the redundant reaction wheel is tilted from its nominal direction by $\Delta\alpha_4$ and $\Delta\beta_4$.

Then, the real control torque acting on spacecrafts with misalignment is expressed as

$$\begin{aligned}\begin{bmatrix}\tau_x\\ \tau_y\\ \tau_z\end{bmatrix} &= \begin{bmatrix}\cos(\Delta\alpha_1)\\ \sin(\Delta\alpha_1)\cos(\Delta\beta_1)\\ \sin(\Delta\alpha_1)\sin(\Delta\beta_1)\end{bmatrix}\tau_1 + \begin{bmatrix}\sin(\Delta\alpha_2)\sin(\Delta\beta_2)\\ \cos(\Delta\alpha_2)\\ \sin(\Delta\alpha_2)\cos(\Delta\beta_2)\end{bmatrix}\tau_2\\ &+ \begin{bmatrix}\sin(\Delta\alpha_3)\cos(\Delta\beta_3)\\ \sin(\Delta\alpha_3)\sin(\Delta\beta_3)\\ \cos(\Delta\alpha_3)\end{bmatrix}\tau_3\\ &+ \begin{bmatrix}\cos(\alpha_4+\Delta\alpha_4)\cos(\beta_4+\Delta\beta_4)\\ \cos(\alpha_4+\Delta\alpha_4)\sin(\beta_4+\Delta\beta_4)\\ \sin(\alpha_4+\Delta\alpha_4)\end{bmatrix}\tau_4.\end{aligned} \tag{16}$$

The definition of the misalignment angles suggests that $\Delta\alpha_i$, $\Delta\beta_i$, $i \in \{1, 2, 3, 4\}$ are small angles. Hence, the following relationships are used to approximate (16):

$$\begin{aligned}\cos(\Delta\alpha_i) &\approx \cos(\Delta\beta_i) \approx 1,\\ \sin(\Delta\alpha_i) &\approx \Delta\alpha_i,\\ \sin(\Delta\beta_i) &\approx \Delta\beta_i.\end{aligned} \tag{17}$$

Then for the considered actuator configuration, the configuration matrix $\mathbf{D}$ can be represented as

$$\mathbf{D} = \mathbf{D}_0 + \Delta\mathbf{D}, \tag{18}$$

where $\mathbf{D}_0$ denotes the nominal configuration matrix, and $\Delta\mathbf{D}$ denotes the actuator misalignment. They can be written as

$$\mathbf{D}_0 = \begin{bmatrix}1 & 0 & 0 & \cos\alpha_4\cos\beta_4\\ 0 & 1 & 0 & \cos\alpha_4\sin\beta_4\\ 0 & 0 & 1 & \sin\alpha_4\end{bmatrix}, \tag{19}$$

$$\begin{aligned}\Delta\mathbf{D} &= \begin{bmatrix}0 & 0 & \Delta\alpha_3 & \Delta\mathbf{D}_{14}\\ \Delta\alpha_1 & 0 & 0 & \Delta\mathbf{D}_{24}\\ 0 & \Delta\alpha_2 & 0 & \Delta\alpha_4\cos\alpha_4\end{bmatrix},\\ \Delta\mathbf{D}_{14} &= -\Delta\alpha_4\sin\alpha_4\cos\beta_4 - \Delta\beta_4\cos\alpha_4\sin\beta_4,\\ \Delta\mathbf{D}_{24} &= -\Delta\alpha_4\sin\alpha_4\sin\beta_4 + \Delta\beta_4\cos\alpha_4\cos\beta_4.\end{aligned} \tag{20}$$

In view of (15) and (18), tracking error dynamics in (12) can be rewritten as

$$\begin{aligned}\mathbf{J}_m\dot{\boldsymbol{\omega}}_e &= -\boldsymbol{\omega}^\times\mathbf{J}_m\boldsymbol{\omega} - \mathbf{J}_m\dot{\boldsymbol{\omega}}_r + \boldsymbol{\delta}^T\mathbf{K}\boldsymbol{\eta} + \boldsymbol{\delta}^T\mathbf{C}\boldsymbol{\psi}\\ &\quad - \boldsymbol{\omega}^\times\boldsymbol{\delta}^T\boldsymbol{\delta}\boldsymbol{\omega} - \boldsymbol{\delta}^T\mathbf{C}\boldsymbol{\delta}\boldsymbol{\omega}_e + (\mathbf{D}_0 + \Delta\mathbf{D})\boldsymbol{\tau} + \mathbf{d}.\end{aligned} \tag{21}$$

To facilitate control system design, the following assumptions and lemmas are presented and will be used in the subsequent developments.

Assumption 1. *The components of external disturbance* $\mathbf{d}$ *in (21) are assumed to be bounded by a set of unknown bounded constants, that is*

$$|\mathbf{d}_i| \le \boldsymbol{\rho}_i\,(i = 1, 2, 3). \tag{22}$$

Assumption 2. *Due to physical limitations on the reaction wheels considered, the maximum output torque of each actuator output torque has the same limit value* ($\underline{\tau}$, $\overline{\tau}$), *that is [29]*

$$\boldsymbol{\tau} \in \Omega = \left\{\tau_i \,\middle|\, \underline{\tau} \le \tau_i \le \overline{\tau},\ i = 1, 2, 3, 4\right\}, \tag{23}$$

where $\underline{\tau}$ *and* $\overline{\tau}$ *represent the known saturation levels of reaction wheels.*

Assumption 3. *The uncertainty* $\Delta\mathbf{D}$ *due to misalignment is an unknown but bounded matrix satisfying*

$$\|\Delta\mathbf{D}\|_F \le \Delta_m, \tag{24}$$

where Δ_m *is a known positive constant.*

Remark 1. According to (20), every element of actuator misalignment matrix $\Delta\mathbf{D}$ is a function of misalignment angle errors which are small in practice, then the Frobenius norm of $\Delta\mathbf{D}$ is bounded by a known quantity Δ_m. It is easy to find a feasible Δ_m in practice.

Lemma 1. *For arbitrary positive constant* ε *and variable* η, *the following inequality holds [30, 31]*

$$0 \le |\eta| - \eta\tanh\left(\frac{\eta}{\varepsilon}\right) \le \kappa\varepsilon, \tag{25}$$

with $\kappa = e^{-(\kappa+1)}$ *and* $\kappa = 0.2785$.

2.4. Control Problem Formulation. Given any initial attitude and angular velocity, the control objective can be stated as considering the flexible spacecraft attitude system described by (1)–(3), design a torque command $\boldsymbol{\tau}$ such that the following goals are met in the presence of uncertain inertia parameters, external disturbance, unmeasured elastic vibration, actuator saturation (23), and even actuator misalignment:

(1) The attitude orientation and angular velocity tracking errors are driven to zero, or a small set containing the origin.

(2) The vibration induced by the maneuver rotation should be attenuated as soon as possible in the presence of parametric uncertainties, external disturbance, actuator saturation, and even actuator misalignment.

3. Robust Adaptive Constrained Controller Design

The proposed attitude control scheme for the flexible spacecraft is shown in Figure 1, in which the controller is composed of an auxiliary design system to compensate the effect of actuator saturation and modal estimator to estimate

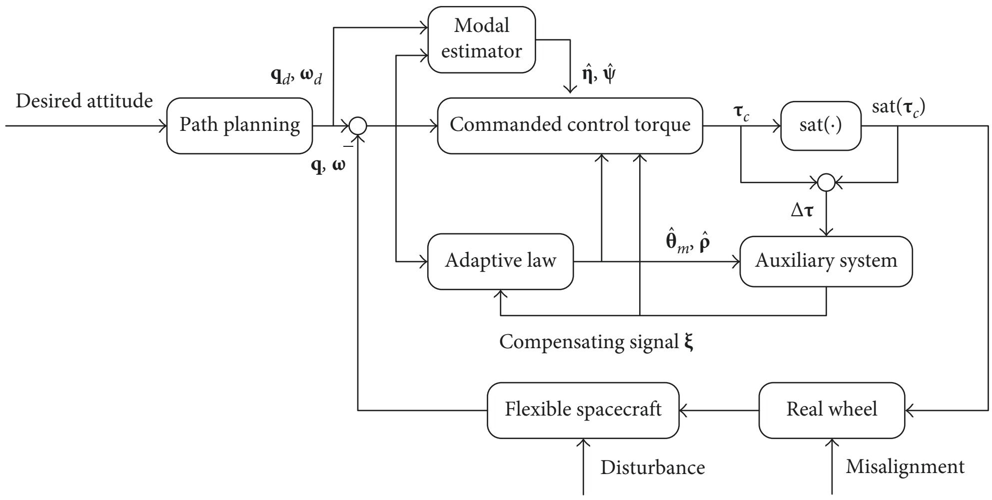

FIGURE 1: Structure of the closed-loop system.

unmeasured modal position and velocity, as well as path planning, which will be given in the following subsections.

3.1. Path Planning. From (2) and (3), it is known that attitude maneuvering would excite appendages' vibration [8], which is closely related to the attitude angular acceleration. A sudden change in attitude signal, especially in the form of step signal, may cause a serious appendages' vibration. Here, in order to achieve high performance of attitude control and attenuate the residual vibration, a novel path planning scheme based on quintic polynomial transition is developed, which is motivated by the previous study of robot trajectory planning in joint space [32]. With regard to the limit of the angular velocity and the angular acceleration, the maneuvering path is designed as follows:

The angular acceleration signal of the path is planned as a quintic polynomial curve.

$$\varphi(t) = a_5 t^5 + a_4 t^4 + a_3 t^3 + a_2 t^2 + a_1 t + a_0. \tag{26}$$

Then, parameters a_5, a_4, a_3, a_2, a_1, and a_0 should be selected appropriately to satisfy the following equality and inequality constraints.

$$\begin{aligned} \varphi(0) &= \varphi_0, \\ \dot{\varphi}(0) &= 0, \\ \ddot{\varphi}(0) &= 0 \\ \varphi(t_f) &= \varphi_f, \\ \dot{\varphi}(t_f) &= 0, \\ \ddot{\varphi}(t_f) &= 0, \end{aligned} \tag{27}$$

$$\begin{aligned} |\dot{\varphi}(t)| &\le \dot{\varphi}_{\max}, \\ |\ddot{\varphi}| &\le \ddot{\varphi}_{\max}, \end{aligned} \tag{28}$$

where $\dot{\varphi}_{\max}$ and $\ddot{\varphi}_{\max}$ are the permitted maximum angular velocity and acceleration, respectively.

Using (27) yields

$$\begin{aligned} a_0 &= \varphi_0, \\ a_1 &= a_2 = 0, \\ a_3 &= \frac{5a_5 t_f^2}{3}, \\ a_4 &= \frac{-5a_5 t_f}{2}. \end{aligned} \tag{29}$$

Angular velocity and acceleration with regard to (26) and (29) are obtained as

$$\begin{aligned} \varphi(t) &= a_5\left(t^5 - \frac{5}{2}t_f t^4 + \frac{5}{3}t_f^2 t^3\right) + \varphi_0, \\ \dot{\varphi}(t) &= a_5\left(5t^4 - 10t_f t^3 + 5t_f^2 t^2\right), \\ \ddot{\varphi}(t) &= a_5\left(20t^3 - 30t_f t^2 + 10t_f^2 t\right). \end{aligned} \tag{30}$$

With the notation $\tau = t/t_f$ and $\hat{a}_5 = a_5 t_f^5$, (30) can be rewritten as

$$\begin{aligned} \varphi(t) &= \hat{a}_5\left(\tau^5 - \frac{5}{2}\tau^4 + \frac{5}{3}\tau^3\right) + \varphi_0, \\ \dot{\overset{\scriptscriptstyle\cdot}{\varphi}}(t) &= \hat{a}_5\left(5\tau^4 - 10\tau^3 + 5\tau^2\right) = t_f\dot{\varphi}(t), \\ \ddot{\overset{\scriptscriptstyle\cdot\cdot}{\varphi}}(t) &= \hat{a}_5\left(20\tau^3 - 30\tau^2 + 10\tau\right) = t_f^2\ddot{\varphi}(t). \end{aligned} \tag{31}$$

For notational convenience, we define $f(\tau)$ as

$$f(\tau) = \tau^5 - \frac{5}{2}\tau^4 + \frac{5}{3}\tau^3, \quad \tau \in [0,\ 1]. \tag{32}$$

It can be easily verified that

$$
\begin{aligned}
&0 \le f(\tau) \le f(1) = \frac{1}{6},\\
&0 \le f'(\tau) \le f'\left(\frac{1}{2}\right) = \frac{5}{16},\\
&f''\left(\frac{1}{2}+\frac{\sqrt{3}}{6}\right) \le f''(\tau) \le f''\left(\frac{1}{2}-\frac{\sqrt{3}}{6}\right),
\end{aligned}
\tag{33}
$$

where

$$
\begin{aligned}
&f''\left(\frac{1}{2}+\frac{\sqrt{3}}{6}\right) = -0.9623,\\
&f''\left(\frac{1}{2}-\frac{\sqrt{3}}{6}\right) = 0.9623.
\end{aligned}
\tag{34}
$$

Then, in view of (27) and (28), $\hat{a}_5$ and t_f satisfy

$$\hat{a}_5 = 6\left(\varphi_f - \varphi_0\right), \tag{35}$$

$$
\begin{aligned}
&t_f \ge \frac{|\dot{\hat{\varphi}}_{\max}|}{\dot{\varphi}_{\max}} = \frac{5|\hat{a}_5|}{16\dot{\varphi}_{\max}},\\
&t_f^2 \ge \frac{|\ddot{\hat{\varphi}}_{\max}|}{\ddot{\varphi}_{\max}} = \frac{0.9623|\hat{a}_5|}{\ddot{\varphi}_{\max}}.
\end{aligned}
\tag{36}
$$

Hence, angular path planning procedure can be described as follows:

(1) Determine $\hat{a}_5$ from (35)
(2) Determine t_f from (36)
(3) Determine a_5, a_4, a_3, a_2, a_1, and a_0 from (29)
(4) Obtain the angular velocity and angular acceleration according to (30).

3.2. Controller Design. To remove the hypothesis of the measurability of the modal position and velocity, an elastic modal estimator to supply their estimates is constructed as follows:

$$\begin{bmatrix}\dot{\hat{\boldsymbol{\eta}}}\\ \dot{\hat{\boldsymbol{\psi}}}\end{bmatrix} = \mathbf{A}\begin{bmatrix}\hat{\boldsymbol{\eta}}\\ \hat{\boldsymbol{\psi}}\end{bmatrix} - \mathbf{AB}\boldsymbol{\delta}\boldsymbol{\omega}_e - \mathbf{B}\boldsymbol{\delta}\dot{\boldsymbol{\omega}}_r, \tag{37}$$

where $\hat{\boldsymbol{\eta}}$, $\hat{\boldsymbol{\psi}}$ are the estimates of modal variables, and $\mathbf{e}_\eta = \boldsymbol{\eta} - \hat{\boldsymbol{\eta}}$, $\mathbf{e}_\psi = \boldsymbol{\psi} - \hat{\boldsymbol{\psi}}$ are their estimation errors.

From (13) and (37), the response of $\mathbf{e}_\eta$, $\mathbf{e}_\psi$ can be algebraically arranged as

$$\begin{bmatrix}\dot{\mathbf{e}}_\eta\\ \dot{\mathbf{e}}_\psi\end{bmatrix} = \mathbf{A}\begin{bmatrix}\mathbf{e}_\eta\\ \mathbf{e}_\psi\end{bmatrix}. \tag{38}$$

Since matrix $\mathbf{A}$ is a Hurwitz matrix, the estimation errors $\mathbf{e}_\eta$, $\mathbf{e}_\psi$ will converge to zero asymptotically.

Considering the actuator saturation in (23), the actual control input $\boldsymbol{\tau} = [\tau_1, \tau_2, \tau_3, \tau_4]^T$ in (21) can be further defined as

$$\tau_i = \operatorname{sat}\left(\tau_{ci}\right) = \begin{cases} \overline{\tau}, & \tau_{ci} > \overline{\tau},\\ \tau_{ci}, & \underline{\tau} \le \tau_{ci} \le \overline{\tau},\\ \underline{\tau}, & \tau_{ci} < \underline{\tau}, \end{cases} \tag{39}$$

where $\boldsymbol{\tau}_c = [\tau_{c1}, \tau_{c2}, \tau_{c3}, \tau_{c4}]^T$ is the desired control input that will be designed in the subsequent developments.

Then, (21) can be rewritten as

$$
\begin{aligned}
\mathbf{J}_m\dot{\boldsymbol{\omega}}_e = {}& -\boldsymbol{\omega}^\times\mathbf{J}_m\boldsymbol{\omega} - \mathbf{J}_m\dot{\boldsymbol{\omega}}_r + \boldsymbol{\delta}^T\mathbf{K}\boldsymbol{\eta} + \boldsymbol{\delta}^T\mathbf{C}\boldsymbol{\psi}\\
& - \boldsymbol{\omega}^\times\boldsymbol{\delta}^T\boldsymbol{\delta}\boldsymbol{\omega} - \boldsymbol{\delta}^T\mathbf{C}\boldsymbol{\delta}\boldsymbol{\omega}_e + \left(\mathbf{D}_0 + \Delta\mathbf{D}\right)\operatorname{sat}\left(\boldsymbol{\tau}_c\right) + \mathbf{d}.
\end{aligned}
\tag{40}
$$

Step 1. We start with (11) and (13) by considering $\boldsymbol{\omega}_e$ as the virtual control variable. Define the tracking error as

$$\mathbf{z} = \boldsymbol{\omega}_e - \boldsymbol{\alpha}_c - \boldsymbol{\xi} = \boldsymbol{\omega}_e - \mathbf{z}_\alpha - \boldsymbol{\alpha} - \boldsymbol{\xi}, \tag{41}$$

where $\boldsymbol{\alpha}_c$ is the output of the following first-order filter utilized to approximate the derivative of the virtual control $\dot{\boldsymbol{\alpha}}$.

$$\boldsymbol{\Gamma}_\alpha\dot{\boldsymbol{\alpha}}_c + \boldsymbol{\alpha}_c = \boldsymbol{\alpha}, \tag{42}$$

where $\boldsymbol{\Gamma}_\alpha = \operatorname{diag}\{\tau_{\alpha 1}, \tau_{\alpha 2}, \tau_{\alpha 3}\}$ is the filter parameter matrix and the components $\boldsymbol{\tau}_{\alpha 1}$, $i = 1, 2, 3$ are positive scalars to be selected. $\mathbf{z}_\alpha = \boldsymbol{\alpha}_c - \boldsymbol{\alpha}$ denotes the estimation error of the filter in (42).

The auxiliary signal $\boldsymbol{\xi}$ in (41) is designed to compensate the effect of actuator saturation and can be produced by the following system:

$$\hat{\mathbf{J}}_m\dot{\boldsymbol{\xi}} = -\mathbf{K}_\xi\boldsymbol{\xi} + \mathbf{D}_0\Delta\boldsymbol{\tau}, \tag{43}$$

where $\mathbf{K}_\xi$ is a positive matrix to be chosen, $\Delta\boldsymbol{\tau}$ denotes the difference between the applied control and the designed control input

$$\Delta\boldsymbol{\tau} = \boldsymbol{\tau} - \boldsymbol{\tau}_c = \operatorname{sat}\left(\boldsymbol{\tau}_c\right) - \boldsymbol{\tau}_c. \tag{44}$$

The first Lyapunov candidate function is chosen as

$$
\begin{aligned}
\mathbf{V}_1 = {}& \left[\left(1 - \mathbf{q}_{e0}\right)^2 + \mathbf{q}_{ev}^T\mathbf{q}_{ev}\right]\\
& + \frac{1}{2}\begin{bmatrix}\hat{\boldsymbol{\eta}}^T & \hat{\boldsymbol{\psi}}^T\end{bmatrix}\mathbf{K}_1\begin{bmatrix}2\mathbf{K}+\mathbf{C}^2 & \mathbf{C}\\ \mathbf{C} & 2\mathbf{I}\end{bmatrix}\begin{bmatrix}\hat{\boldsymbol{\eta}}\\ \hat{\boldsymbol{\psi}}\end{bmatrix}\\
& + \frac{1}{2}\begin{bmatrix}\mathbf{e}_\eta^T & \mathbf{e}_\psi^T\end{bmatrix}\mathbf{K}_2\begin{bmatrix}2\mathbf{K}+\mathbf{C}^2 & \mathbf{C}\\ \mathbf{C} & 2\mathbf{I}\end{bmatrix}\begin{bmatrix}\mathbf{e}_\eta\\ \mathbf{e}_\psi\end{bmatrix},
\end{aligned}
\tag{45}
$$

where the positive definite matrices $\mathbf{K}_1$ and $\mathbf{K}_2$ are partitioned as

$$
\begin{aligned}
\mathbf{K}_1 &= \begin{bmatrix}k_{11}\mathbf{I} & 0\\ 0 & k_{12}\mathbf{I}\end{bmatrix},\\
\mathbf{K}_2 &= \begin{bmatrix}k_{21}\mathbf{I} & 0\\ 0 & k_{22}\mathbf{I}\end{bmatrix}.
\end{aligned}
\tag{46}
$$

Using (11), (37), (38) and (41), the time derivative of (45) is given by

$$\begin{aligned}\dot{\mathbf{V}}_1 &= \mathbf{x}^T\boldsymbol{\omega}_e - \mathbf{y} - \begin{bmatrix}\hat{\boldsymbol{\eta}}^T & \hat{\boldsymbol{\psi}}^T\end{bmatrix}\begin{bmatrix}k_{11}\mathbf{CK} & -2k_{11}\mathbf{K}\\ 2k_{12}\mathbf{K} & k_{12}\mathbf{C}\end{bmatrix}\begin{bmatrix}\hat{\boldsymbol{\eta}}\\ \hat{\boldsymbol{\psi}}\end{bmatrix}\\ &\quad - \begin{bmatrix}\mathbf{e}_\eta^T & \mathbf{e}_\psi^T\end{bmatrix}\begin{bmatrix}k_{21}\mathbf{CK} & -2k_{21}K\\ 2k_{22}\mathbf{K} & k_{22}\mathbf{C}\end{bmatrix}\begin{bmatrix}\mathbf{e}_\eta\\ \mathbf{e}_\psi\end{bmatrix}\\ &= \mathbf{x}^T\left(\mathbf{z} + \mathbf{z}_\alpha + \boldsymbol{\alpha} + \boldsymbol{\xi}\right) - \mathbf{y}\\ &\quad - \begin{bmatrix}\hat{\boldsymbol{\eta}}^T & \hat{\boldsymbol{\psi}}^T\end{bmatrix}\begin{bmatrix}k_{11}\mathbf{CK} & -2k_{11}\mathbf{K}\\ 2k_{12}\mathbf{K} & k_{12}\mathbf{C}\end{bmatrix}\begin{bmatrix}\hat{\boldsymbol{\eta}}\\ \hat{\boldsymbol{\psi}}\end{bmatrix}\\ &\quad - \begin{bmatrix}\mathbf{e}_\eta^T & \mathbf{e}_\psi^T\end{bmatrix}\begin{bmatrix}k_{21}\mathbf{CK} & -2k_{21}\mathbf{K}\\ 2k_{22}\mathbf{K} & k_{22}\mathbf{C}\end{bmatrix}\begin{bmatrix}\mathbf{e}_\eta\\ \mathbf{e}_\psi\end{bmatrix},\end{aligned} \tag{47}$$

where $\mathbf{x}$ and $\mathbf{y}$ are defined as

$$\begin{aligned}\mathbf{x}^T &= \mathbf{q}_{ev}^T + \left(k_{12}\hat{\boldsymbol{\psi}}^T\mathbf{C} - 2k_{11}\hat{\boldsymbol{\eta}}^T\mathbf{K}\right)\boldsymbol{\delta}\\ &\quad - \left(k_{11}\hat{\boldsymbol{\eta}}^T\mathbf{C} + 2k_{12}\hat{\boldsymbol{\psi}}^T\right)\boldsymbol{\delta}\mathbf{S}\left(\mathbf{R}\left(\mathbf{q}_e\right)\boldsymbol{\omega}_d\right),\\ \mathbf{y} &= \left(k_{11}\hat{\boldsymbol{\eta}}^T\mathbf{C} + 2k_{12}\hat{\boldsymbol{\psi}}^T\right)\boldsymbol{\delta}\mathbf{R}\left(\mathbf{q}_e\right)\dot{\boldsymbol{\omega}}_d.\end{aligned} \tag{48}$$

Define the virtual control $\boldsymbol{\alpha}$ as

$$\boldsymbol{\alpha} = -\mathbf{K}_3\mathbf{x} - \boldsymbol{\xi} + \frac{\operatorname{sgn}(\mathbf{x})}{\|\mathbf{x}\|_1}\mathbf{y}. \tag{49}$$

Based on what is mentioned above, (47) be rewritten as

$$\begin{aligned}\dot{\mathbf{V}}_1 &= \mathbf{x}^T\mathbf{z} + \mathbf{x}^T\mathbf{z}_\alpha - \mathbf{x}^T\mathbf{K}_3\mathbf{x} - \begin{bmatrix}\hat{\boldsymbol{\eta}}^T & \hat{\boldsymbol{\psi}}^T\end{bmatrix}\begin{bmatrix}k_{11}\mathbf{CK} & -2k_{11}\mathbf{K}\\ 2k_{12}\mathbf{K} & k_{12}\mathbf{C}\end{bmatrix}\begin{bmatrix}\hat{\boldsymbol{\eta}}\\ \hat{\boldsymbol{\psi}}\end{bmatrix}\\ &\quad - \begin{bmatrix}\mathbf{e}_\eta^T & \mathbf{e}_\psi^T\end{bmatrix}\begin{bmatrix}k_{21}\mathbf{CK} & -2k_{21}\mathbf{K}\\ 2k_{22}\mathbf{K} & k_{22}\mathbf{C}\end{bmatrix}\begin{bmatrix}\mathbf{e}_\eta\\ \mathbf{e}_\psi\end{bmatrix}.\end{aligned} \tag{50}$$

Step 2. Take the derivate of $\mathbf{z}$ left-multiplied by inertia matrix with respect to (40), then we have

$$\begin{aligned}\mathbf{J}_m\dot{\mathbf{z}} &= -\boldsymbol{\omega}^\times\mathbf{J}_m\boldsymbol{\omega} - \mathbf{J}_m\dot{\boldsymbol{\omega}}_r + \boldsymbol{\delta}^T\mathbf{K}\boldsymbol{\eta} + \boldsymbol{\delta}^T\mathbf{C}\boldsymbol{\psi} - \boldsymbol{\omega}^\times\boldsymbol{\delta}^T\boldsymbol{\delta}\boldsymbol{\omega} - \boldsymbol{\delta}^T\mathbf{C}\boldsymbol{\delta}\boldsymbol{\omega}_e\\ &\quad + \mathbf{D}_0\operatorname{sat}\left(\boldsymbol{\tau}_c\right) + \Delta\mathbf{D}\operatorname{sat}\left(\boldsymbol{\tau}_c\right) + \mathbf{d} - \mathbf{J}_m\dot{\boldsymbol{\alpha}}_c - \mathbf{J}_m\dot{\boldsymbol{\xi}}.\end{aligned} \tag{51}$$

Although the inertia matrix is unknown for the system design, it can be observed that the inertia parameters appear linearly in (51). To isolate these parameters, a linear operator $\mathbf{L}(\cdot)$: $\mathbb{R}^3 \to \mathbb{R}^{3\times 6}$ acting on $\mathbf{a} = \begin{bmatrix}a_1 & a_2 & a_3\end{bmatrix}^T$ is introduced as follows

$$\mathbf{L}(\mathbf{a}) = \begin{bmatrix}a_1 & 0 & 0 & a_2 & a_3 & 0\\ 0 & a_2 & 0 & a_1 & 0 & a_3\\ 0 & 0 & a_3 & 0 & a_1 & a_2\end{bmatrix}. \tag{52}$$

Let $\boldsymbol{\theta}_m^T = [J_{m,11}, J_{m,22}, J_{m,33}, J_{m,12}, J_{m,13}, J_{m,23}]$, it follows that $\mathbf{J}_m\mathbf{a} = L(\mathbf{a})\boldsymbol{\theta}_m$ and then (51) can be rewritten as

$$\begin{aligned}\mathbf{J}_m\dot{\mathbf{z}} &= \mathbf{F}_1\boldsymbol{\theta}_m + \mathbf{L}(\dot{\boldsymbol{\xi}})\tilde{\boldsymbol{\theta}}_m + \boldsymbol{\delta}^T\mathbf{K}\boldsymbol{\eta} + \boldsymbol{\delta}^T\mathbf{C}\boldsymbol{\psi} - \boldsymbol{\omega}^\times\boldsymbol{\delta}^T\boldsymbol{\delta}\boldsymbol{\omega} - \boldsymbol{\delta}^T\mathbf{C}\boldsymbol{\delta}\boldsymbol{\omega}_e\\ &\quad + \Delta\mathbf{D}\operatorname{sat}\left(\boldsymbol{\tau}_c\right) + \mathbf{D}_0\boldsymbol{\tau}_c + \mathbf{d} + \mathbf{K}_\xi\boldsymbol{\xi},\end{aligned} \tag{53}$$

with $\mathbf{F}_1 = -\boldsymbol{\omega}^\times\mathbf{L}(\boldsymbol{\omega}) - \mathbf{L}(\dot{\boldsymbol{\omega}}_r) - \mathbf{L}(\dot{\boldsymbol{\alpha}}_c)$. $\tilde{\boldsymbol{\theta}}_m$ denotes the estimate error of $\boldsymbol{\theta}_m$ and is defined as $\tilde{\boldsymbol{\theta}}_m = \hat{\boldsymbol{\theta}}_m - \boldsymbol{\theta}_m$.

The design procedure can be summarized in the following theorem.

Theorem 1. *Consider the flexible spacecraft system involving uncertain inertia parameters, external disturbance, unmeasured elastic vibration, actuator saturation, and even actuator misalignment. If the control law is designed by*

$$\begin{aligned}\boldsymbol{\tau}_c &= -\mathbf{D}_0^+\left(\mathbf{x} + \mathbf{K}_\xi\boldsymbol{\xi} + \mathbf{K}_4\mathbf{z}\right) - \mathbf{D}_0^+\mathbf{F}_1\hat{\boldsymbol{\theta}}_{mb}\\ &\quad - \mathbf{D}_0^+\left(\boldsymbol{\delta}^T\mathbf{K}\hat{\boldsymbol{\eta}} + \boldsymbol{\delta}^T\mathbf{C}\hat{\boldsymbol{\psi}} - \boldsymbol{\omega}^\times\boldsymbol{\delta}^T\boldsymbol{\delta}\boldsymbol{\omega} - \boldsymbol{\delta}^T\mathbf{C}\boldsymbol{\delta}\boldsymbol{\omega}_e\right)\\ &\quad - \frac{1}{2}\mathbf{D}_0^+\left[(\mathbf{K}\boldsymbol{\delta})^T(\mathbf{K}\boldsymbol{\delta}\mathbf{z}) + (\mathbf{C}\boldsymbol{\delta})^T(\mathbf{C}\boldsymbol{\delta}\mathbf{z})\right]\\ &\quad - 2\mathbf{D}_0^+\Delta_m\tau_m\tanh\left(\frac{2\Delta_m\tau_m\mathbf{z}}{\varepsilon}\right) - \mathbf{D}_0^+\tanh(\mathbf{z})\hat{\boldsymbol{\rho}},\end{aligned} \tag{54}$$

where $\tanh(\mathbf{z}) = \operatorname{diag}(\tanh(\mathbf{z}_j/\varepsilon_{dj}))$, *the adaptive control is selected as*

$$\begin{aligned}\dot{\hat{\boldsymbol{\theta}}}_m &= \operatorname{Proj}\left(\boldsymbol{\Gamma}_1\mathbf{F}_2^T\mathbf{z}\right),\\ \dot{\hat{\boldsymbol{\rho}}} &= \boldsymbol{\Gamma}_2\left(\tanh(\mathbf{z})\mathbf{z} - \mathbf{k}_\rho\hat{\boldsymbol{\rho}}\right),\end{aligned} \tag{55}$$

where $\mathbf{F}_2 = \mathbf{F}_1 - \mathbf{L}(\dot{\boldsymbol{\xi}})$, *the projection operator Proj$(\cdot)$ is defined in [33] to avoid the parameter drift problem, then the attitude orientation and angular velocity tracking errors are uniformly ultimately bounded.*

Proof. Consider the composite Lyapunov function V_2 as

$$V_2 = V_1 + \frac{1}{2}\mathbf{z}^T\mathbf{J}_m\mathbf{z} + \frac{1}{2}\tilde{\boldsymbol{\theta}}_m^T\boldsymbol{\Gamma}_1^{-1}\tilde{\boldsymbol{\theta}}_m + \frac{1}{2}\tilde{\boldsymbol{\rho}}^T\boldsymbol{\Gamma}_2^{-1}\tilde{\boldsymbol{\rho}}. \tag{56}$$

Substituting the aforementioned control torque (54), taking the derivative of the above Lyapunov function with regard to (50) and (53), it follows

$$\begin{aligned}\dot{V}_2 &= -\mathbf{x}^T\mathbf{K}_3\mathbf{x} - \mathbf{z}^T\mathbf{K}_4\mathbf{z} + \mathbf{x}^T\mathbf{z}_\alpha\\ &\quad - \begin{bmatrix}\hat{\boldsymbol{\eta}}^T & \hat{\boldsymbol{\psi}}^T\end{bmatrix}\begin{bmatrix}k_{11}\mathbf{CK} & -2k_{11}\mathbf{K}\\ 2k_{12}\mathbf{K} & k_{12}\mathbf{C}\end{bmatrix}\begin{bmatrix}\hat{\boldsymbol{\eta}}\\ \hat{\boldsymbol{\psi}}\end{bmatrix}\\ &\quad - \begin{bmatrix}\mathbf{e}_\eta^T & \mathbf{e}_\psi^T\end{bmatrix}\begin{bmatrix}k_{21}\mathbf{CK} & -2k_{21}\mathbf{K}\\ 2k_{22}\mathbf{K} & k_{22}\mathbf{C}\end{bmatrix}\begin{bmatrix}\mathbf{e}_\eta\\ \mathbf{e}_\psi\end{bmatrix}\\ &\quad + \left[\tilde{\boldsymbol{\theta}}_m^T\boldsymbol{\Gamma}_1^{-1}\dot{\hat{\boldsymbol{\theta}}}_{mb} - \mathbf{z}^T\mathbf{F}_2\tilde{\boldsymbol{\theta}}_m\right]\\ &\quad + \left[\tilde{\boldsymbol{\rho}}^T\boldsymbol{\Gamma}_2^{-1}\dot{\hat{\boldsymbol{\rho}}} + \mathbf{z}^T\mathbf{d} - \mathbf{z}^T\tanh(\mathbf{z})\hat{\boldsymbol{\rho}}\right]\\ &\quad + \left[\mathbf{z}^T\Delta\mathbf{D}\operatorname{sat}\left(\boldsymbol{\tau}_c\right) - 2\Delta_m\tau_m\mathbf{z}^T\tanh\left(\frac{2\Delta_m\tau_m\mathbf{z}}{\varepsilon}\right)\right]\\ &\quad + \left[\mathbf{z}^T\boldsymbol{\delta}^T\mathbf{K}\mathbf{e}_\eta - \frac{1}{2}(\mathbf{K}\boldsymbol{\delta}\mathbf{z})^T(\mathbf{K}\boldsymbol{\delta}\mathbf{z})\right]\\ &\quad + \left[\mathbf{z}^T\boldsymbol{\delta}^T\mathbf{C}\mathbf{e}_\psi - \frac{1}{2}(\mathbf{C}\boldsymbol{\delta}\mathbf{z})^T(\mathbf{C}\boldsymbol{\delta}\mathbf{z})\right].\end{aligned} \tag{57}$$

In view of the conclusion in [34], we have $\|\mathbf{z}_\alpha\| \le \mu$, then

$$-\mathbf{x}^T\mathbf{K}_3\mathbf{x} + \mathbf{x}^T\mathbf{z}_\alpha \le -\mathbf{x}^T\left(\mathbf{K}_3 - \frac{1}{2}\mathbf{I}\right)\mathbf{x} + \frac{1}{2}\mu^2. \quad (58)$$

The last two terms in (57) can be expanded as

$$\begin{aligned}\mathbf{z}^T\boldsymbol{\delta}^T\mathbf{K}\mathbf{e}_\eta - \frac{1}{2}(\mathbf{K}\boldsymbol{\delta}\mathbf{z})^T(\mathbf{K}\boldsymbol{\delta}\mathbf{z}) &\le \frac{1}{2}\mathbf{e}_\eta^T\mathbf{e}_\eta,\\ \mathbf{z}^T\boldsymbol{\delta}^T\mathbf{C}\mathbf{e}_\psi - \frac{1}{2}(\mathbf{C}\boldsymbol{\delta}\mathbf{z})^T(\mathbf{C}\boldsymbol{\delta}\mathbf{z}) &\le \frac{1}{2}\mathbf{e}_\psi^T\mathbf{e}_\psi.\end{aligned} \quad (59)$$

According to Lemma 1, we have

$$\begin{aligned}\sum_{j=1}^{3}\left|\mathbf{z}_j\right|\left|\boldsymbol{\rho}_j\right| &\le \sum_{j=1}^{3}\left(\kappa_{dj}\varepsilon_{dj} + \mathbf{z}_j\tanh\left(\frac{\mathbf{z}_j}{\varepsilon_{dj}}\right)\right)\boldsymbol{\rho}_j\\ &= \boldsymbol{\varphi}^T\boldsymbol{\rho} + \mathbf{z}^T\tanh(\mathbf{z})\boldsymbol{\rho}\\ &\le \frac{\|\boldsymbol{\varphi}\|^2}{2} + \frac{\|\boldsymbol{\rho}\|^2}{2} + \mathbf{z}^T\tanh(\mathbf{z})\boldsymbol{\rho},\end{aligned} \quad (60)$$

where

$$\begin{aligned}\boldsymbol{\varphi} &= \left[\kappa\varepsilon_{d1}, \ \kappa\varepsilon_{d2}, \ \kappa\varepsilon_{d3}\right]^T,\\ \boldsymbol{\rho} &= \left[\rho_1, \ \rho_2, \ \rho_3\right]^T.\end{aligned} \quad (61)$$

Then, substituting the aforementioned adaptive law and considering the property of projection operator as well as the following inequality

$$-\tilde{\boldsymbol{\rho}}^T\hat{\boldsymbol{\rho}} \le -\frac{1}{2}\|\tilde{\boldsymbol{\rho}}\|^2 + \frac{1}{2}\|\boldsymbol{\rho}\|^2, \quad (62)$$

gives

$$\begin{aligned}&\tilde{\boldsymbol{\theta}}_m^T\boldsymbol{\Gamma}_1^{-1}\dot{\hat{\boldsymbol{\theta}}}_m - \mathbf{z}^T\mathbf{F}_2\tilde{\boldsymbol{\theta}}_m \le 0,\\ &\tilde{\boldsymbol{\rho}}^T\boldsymbol{\Gamma}_2^{-1}\dot{\hat{\boldsymbol{\rho}}} + \mathbf{z}^T\mathbf{d} - \mathbf{z}^T\tanh(\mathbf{z})\hat{\boldsymbol{\rho}} \le -\frac{k_\rho}{2}\|\tilde{\boldsymbol{\rho}}\|^2 + \frac{\|\boldsymbol{\varphi}\|^2}{2} + \frac{\left(1 + k_\rho\right)}{2}\|\boldsymbol{\rho}\|^2.\end{aligned} \quad (63)$$

Assumption 2 dictates that $\|\mathrm{sat}(\boldsymbol{\tau}_c)\| \le 2\tau_m$, τ_m is the permitted maximum control torque. Combining Assumption 2 and Lemma 1 yields to

$$\mathbf{z}^T\Delta\mathbf{D}\ \mathrm{sat}\left(\boldsymbol{\tau}_c\right) - 2\Delta_m\tau_m\mathbf{z}^T\tanh\left(\frac{2\Delta_m\tau_m\mathbf{z}}{\varepsilon}\right) \le 3\kappa\varepsilon. \quad (64)$$

From the above development, (57) can be further derived as

$$\begin{aligned}\dot{V}_2 = &-\mathbf{z}^T\mathbf{K}_4\mathbf{z} - \mathbf{x}^T\left(\mathbf{K}_3 - \frac{1}{2}\mathbf{I}\right)\mathbf{x} - \frac{k_\rho}{2}\|\tilde{\boldsymbol{\rho}}\|^2\\ &- \left[\hat{\boldsymbol{\eta}}^T \ \ \hat{\boldsymbol{\psi}}^T\right]\begin{bmatrix}k_{11}\mathbf{C}\mathbf{K} & -2k_{11}\mathbf{K}\\ 2k_{12}\mathbf{K} & k_{12}\mathbf{C}\end{bmatrix}\begin{bmatrix}\hat{\boldsymbol{\eta}}\\ \hat{\boldsymbol{\psi}}\end{bmatrix}\\ &- \left[\mathbf{e}_\eta^T \ \ \mathbf{e}_\psi^T\right]\begin{bmatrix}k_{21}\mathbf{C}\mathbf{K} & -2k_{21}\mathbf{K}\\ 2k_{22}\mathbf{K} & k_{22}\mathbf{C}\end{bmatrix}\begin{bmatrix}\mathbf{e}_\eta\\ \mathbf{e}_\psi\end{bmatrix}\\ &+ \frac{\|\boldsymbol{\varphi}\|^2}{2} + \frac{\left(1 + k_\rho\right)}{2}\|\boldsymbol{\rho}\|^2 + \frac{1}{2}\mu^2 + 3\kappa\varepsilon.\end{aligned} \quad (65)$$

If parameters $\mathbf{K}_1$, $\mathbf{K}_2$, and $\mathbf{K}_3$ are selected such that

$$\begin{aligned}\bar{\mathbf{K}}_1 &= \begin{bmatrix}k_{11}\mathbf{C}\mathbf{K} & -2k_{11}\mathbf{K}\\ 2k_{12}\mathbf{K} & k_{12}\mathbf{C}\end{bmatrix} > 0,\\ \bar{\mathbf{K}}_2 &= \begin{bmatrix}k_{21}\mathbf{C}\mathbf{K} & -2k_{21}\mathbf{K}\\ 2k_{22}\mathbf{K} & k_{22}\mathbf{C}\end{bmatrix} > 0,\\ \bar{\mathbf{K}}_3 &= \mathbf{K}_3 - \frac{1}{2}\mathbf{I} > 0,\end{aligned} \quad (66)$$

then $\dot{V}_2$ can be further upper bounded by

$$\dot{V}_2 \le -kV_2 + \varepsilon_t, \quad (67)$$

where ε_t is given by

$$\varepsilon_t = \frac{\|\boldsymbol{\varphi}\|^2}{2} + \frac{1 + k_\rho}{2\|\boldsymbol{\rho}\|^2} + \frac{1}{2}\mu^2 + 3\kappa\varepsilon, \quad (68)$$

which readily concludes that

$$0 \le V_2(t) \le \left(\frac{\varepsilon_t}{k}\right) + \left(V_2(0) - \left(\frac{\varepsilon_t}{k}\right)\right)e^{-kt}. \quad (69)$$

Hence, V_2 is bounded. It follows the definition of V_2 that the quaternion tracking error $\mathbf{q}_{ev}$, angular velocity control error $\mathbf{z}$, modal variables estimates $[\hat{\boldsymbol{\eta}}^T, \ \hat{\boldsymbol{\psi}}^T]^T$, and parameter estimation error $\tilde{\boldsymbol{\theta}}_m$ are all bounded. Therefore, the controlled closed-loop system is uniformly ultimately bounded.

In addition, following the definition of V_2 also yields

$$\begin{aligned}\max\left\{\mathbf{q}_{ev}^T\mathbf{q}_{ev}, \ \frac{1}{2}\lambda_{\min}(\mathbf{J})\mathbf{z}^T\mathbf{z}\right\} \le V_2(t) &\le \left(\frac{\varepsilon_t}{k}\right)\\ &+ \left(V_2(0) - \left(\frac{\varepsilon_t}{k}\right)\right)e^{-kt},\end{aligned} \quad (70)$$

such that quaternion tracking error $\mathbf{q}_{ev}$ and angular velocity control error $\mathbf{z}$, respectively, converge to the following compact sets:

$$\begin{aligned}\Omega_1 &= \left\{\mathbf{q}_{ev}\ \middle|\ \|\mathbf{q}_{ev}\| \le \sqrt{\frac{\varepsilon_t}{k}}\right\},\\ \Omega_2 &= \left\{\mathbf{z}\ \middle|\ \|\mathbf{z}\| \le \sqrt{\frac{2\varepsilon_t}{k\lambda_{\min}(\mathbf{J})}}\right\}.\end{aligned} \quad (71)$$

According to (41), the angular velocity tracking error $\boldsymbol{\omega}_e$ is also uniformly ultimately bounded. The convergence domain Ω_1 and Ω_2 can be adjusted by an explicit choice of design parameters. □

4. Numerical Simulation

Numerical simulations have been carried out in this section to illustrate and verify the effectiveness of the proposed control scheme. The spacecraft is characterized by a nominal main body inertia matrix

$$\mathbf{J} = \begin{bmatrix}350 & 3 & 4\\ 3 & 280 & 10\\ 4 & 10 & 190\end{bmatrix}\ \mathrm{kg{\cdot}m^2}, \quad (72)$$

and by the coupling matrix

$$\boldsymbol{\delta} = \begin{bmatrix} 6.45637 & 1.27814 & 2.15629 \\ -1.25619 & 0.91756 & -1.67264 \\ 1.11687 & 2.48901 & -0.83674 \\ 1.23637 & -2.6581 & -1.12503 \end{bmatrix} \mathrm{kg}^{1/2}\cdot\mathrm{m}, \tag{73}$$

respectively. Then matrix $\mathbf{J}_m$ is given by

$$\mathbf{J}_m = \begin{bmatrix} 303.9613 & -3.5930 & -9.6975 \\ -3.5930 & 264.2638 & 7.8709 \\ -9.6975 & 7.8709 & 180.5869 \end{bmatrix} \mathrm{kg}\cdot\mathrm{m}^2 \tag{74}$$

The first four elastic modes have been taken into account for the implemented spacecraft model resulting from the modal analysis of the structure, with natural frequency and damping presented in Table 1.

The maximum angular velocity and acceleration of the flexible spacecraft are $v_{\max} = 0.0343$ rad/s and $a_{\max} = 0.0286$ rad/s^2, respectively. Herein, we consider a three-axis large angle maneuver. The initial attitude in Euler angles is $[0^\circ\ \ 30^\circ\ \ 45^\circ]^T$, and the corresponding initial attitude in quaternion is $\mathbf{q}^T(0) = [0.8924,\ -0.0990,\ 0.2391,\ 0.3696]$. The desired attitude is $[30^\circ\ \ 45^\circ\ \ 60^\circ]^T$. The initial and desired angular velocity are chosen to be $\boldsymbol{\omega}^T(0) = [0,\ 0,\ 0]$. Sample time is $t_s = 0.01$ s, and the span of simulation time is from 0 to 200 s. In addition, the initial modal variables and its time derivative are given by

$$\boldsymbol{\eta}^T(0) = [0.01242,\ 0.01584,\ -0.01749,\ 0.01125], \tag{75}$$

and $\dot{\boldsymbol{\eta}}^T(0) = [0,\ 0,\ 0,\ 0]$, respectively.

To examine the robustness to external disturbance, simulation is done corresponding to the following periodic disturbance torque

$$\mathbf{d}(t) = \begin{bmatrix} 0.03\cos(0.01t) + 0.01 \\ 0.015\sin(0.02t) + 0.03\cos(0.025t) \\ 0.03\sin(0.01t) + 0.01 \end{bmatrix} \mathrm{Nm}. \tag{76}$$

For the purpose of comparison, two different sets of simulation are conducted to demonstrate the effectiveness of the proposed control approach as follows:

Case 1. Attitude control without considering the actuator saturation and even actuator misalignment. The robust adaptive control (RAC) law and corresponding adaptive law are derived in steps identical to those employed in Section 3.2 as

$$\begin{aligned} \boldsymbol{\tau}_c = &-\mathbf{D}_0^{+}(\mathbf{x} + \mathbf{K}_4\mathbf{z}) - \mathbf{D}_0^{+}\mathbf{F}_1\hat{\boldsymbol{\theta}}_{mb} \\ &- \mathbf{D}_0^{+}\left(\boldsymbol{\delta}^T\mathbf{K}\hat{\boldsymbol{\eta}} + \boldsymbol{\delta}^T\mathbf{C}\hat{\boldsymbol{\psi}} - \boldsymbol{\omega}^{\times}\boldsymbol{\delta}^T\boldsymbol{\delta}\boldsymbol{\omega} - \boldsymbol{\delta}^T\mathbf{C}\boldsymbol{\delta}\boldsymbol{\omega}_e\right) \\ &- \frac{1}{2}\mathbf{D}_0^{+}\left[(\mathbf{K}\boldsymbol{\delta})^T(\mathbf{K}\boldsymbol{\delta}\mathbf{z}) + (\mathbf{C}\boldsymbol{\delta})^T(\mathbf{C}\boldsymbol{\delta}\mathbf{z})\right] - \mathbf{D}_0^{+}\tanh(\mathbf{z})\hat{\boldsymbol{\rho}}, \end{aligned} \tag{77}$$

$$\begin{aligned} \dot{\hat{\boldsymbol{\theta}}}_m &= \mathrm{Proj}\left(\boldsymbol{\Gamma}_1\mathbf{F}_1^T\mathbf{z}\right), \\ \dot{\hat{\boldsymbol{\rho}}} &= \boldsymbol{\Gamma}_2\left(\tanh(\mathbf{z})\mathbf{z} - k_\rho\hat{\boldsymbol{\rho}}\right). \end{aligned} \tag{78}$$

Table 1: Parameters of the flexible dynamics.

	Natural frequency (rad/s)	Damping
Mode 1	1.0973	0.05
Mode 2	1.2761	0.06
Mode 3	1.6538	0.08
Mode 4	2.2893	0.025

Table 2: Design parameters for the different controllers.

Control schemes	Parameters and values
Proposed controller in (77) and (78)	$k_{11} = k_{12} = 0.1,\ k_{21} = 4, k_{22} = 5,$ $\mathbf{K}_3 = 0.55\mathbf{I}_3,\ \mathbf{K}_4 = 0.1\mathbf{I}_3,$ $\boldsymbol{\Gamma}_\alpha = 0.01\mathbf{I}_3,\ \boldsymbol{\Gamma}_1 = 0.01I_6,\ \boldsymbol{\Gamma}_2 = 0.01\mathbf{I}_3,$ $k_\rho = 0.001,\ \varepsilon_d = 0.01,$
Proposed controller in (54) and (55)	$k_{11} = k_{12} = 0.1,\ k_{21} = 4, k_{22} = 5,$ $\mathbf{K}_3 = 0.55\mathbf{I}_3,\ \mathbf{K}_4 = 0.1\mathbf{I}_3,\ \mathbf{K}_\xi = 0.3\mathbf{I}_3,$ $\boldsymbol{\Gamma}_\alpha = 0.01\mathbf{I}_3,\ \boldsymbol{\Gamma}_1 = 0.01\mathbf{I}_6,\ \boldsymbol{\Gamma}_2 = 0.01\mathbf{I}_3,$ $k_\rho = 0.001,\ \varepsilon_d = 0.01,\ \varepsilon = 0.01,\ \tau_m = 10,$

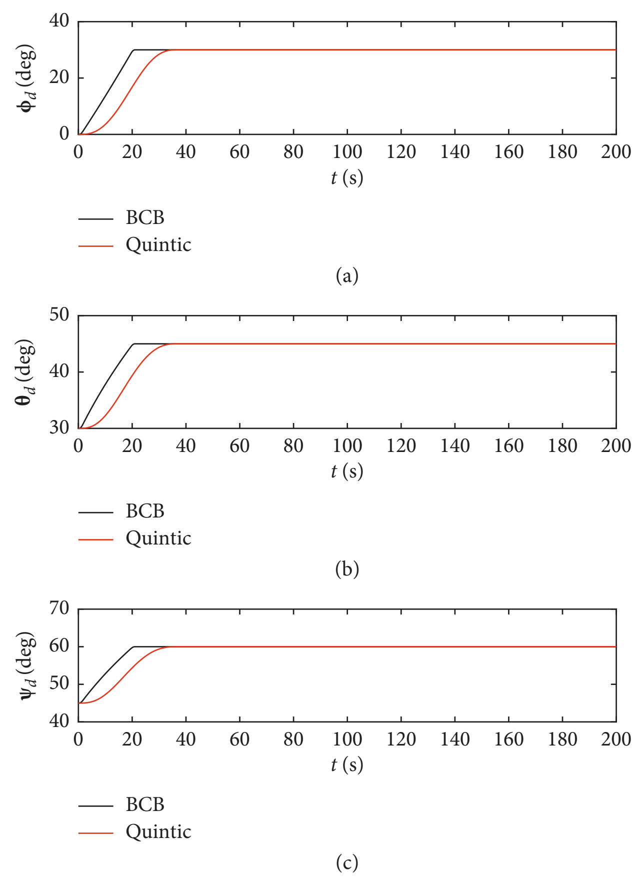

Figure 2: Time response of planned attitude path.

Case 2. Attitude control using constrained robust adaptive control (CRAC) law (54) and adaptive law (55), taking actuator saturation and even actuator misalignment into account explicitly.

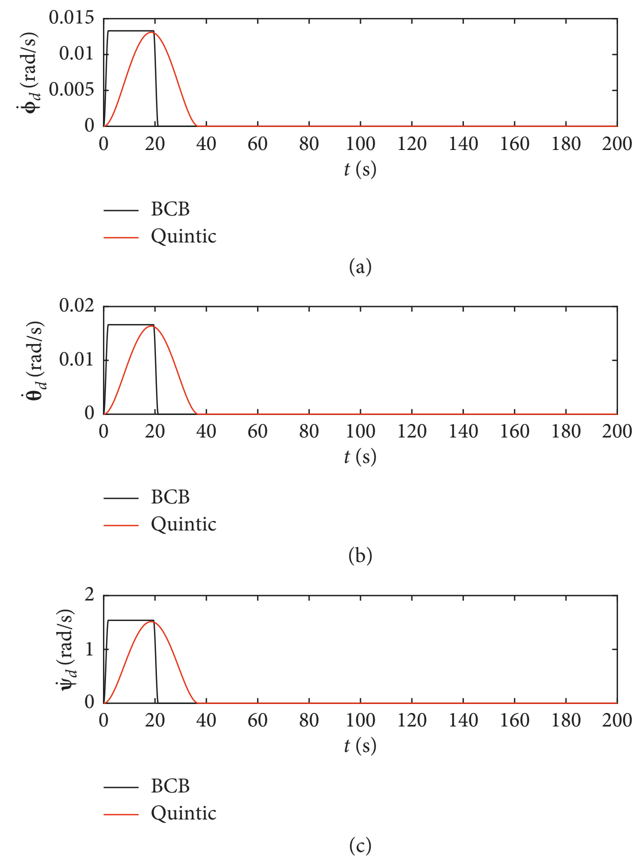

Figure 3: Time response of planned angular velocity.

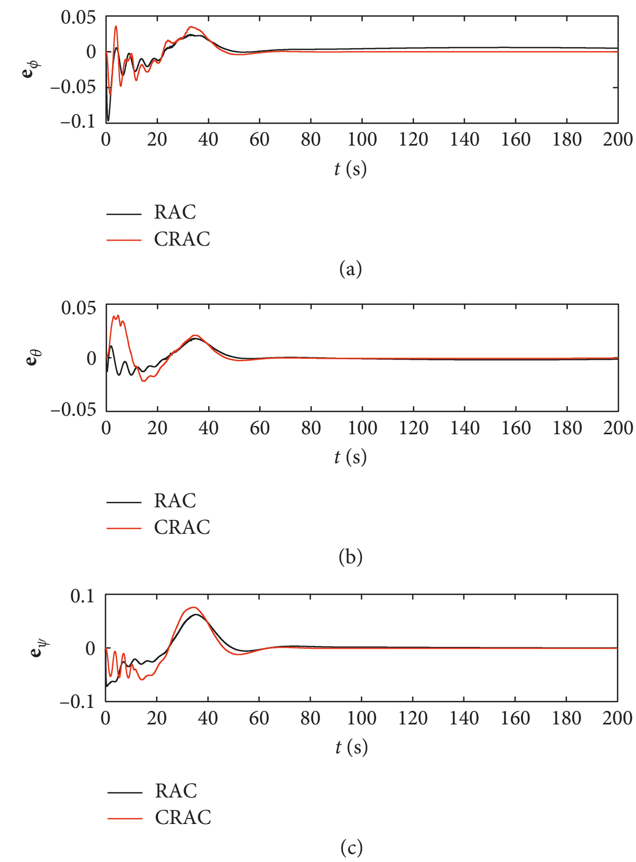

Figure 5: Time response of attitude tracking error in Euler angle.

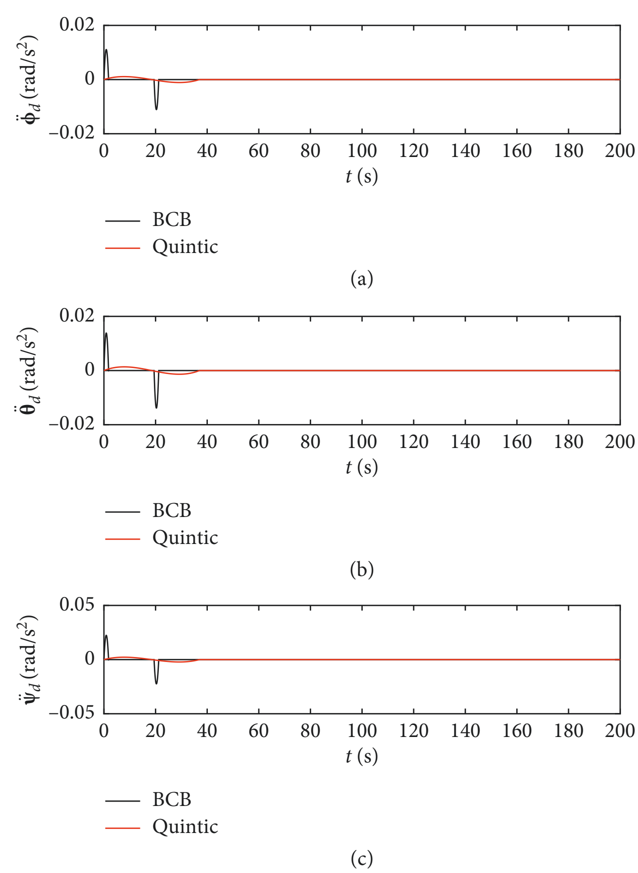

Figure 4: Time response of planned angular acceleration.

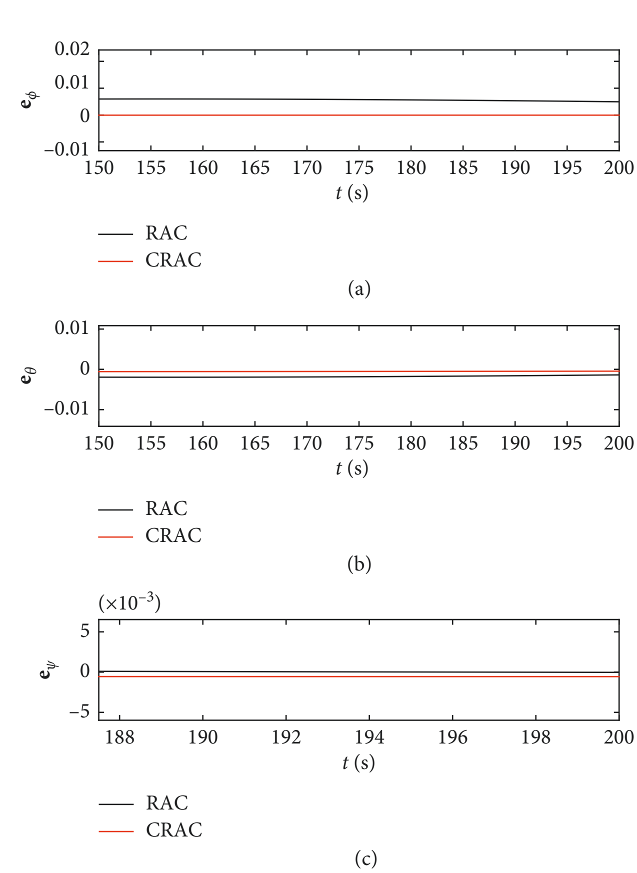

Figure 6: Enlarged version of Figure 5.

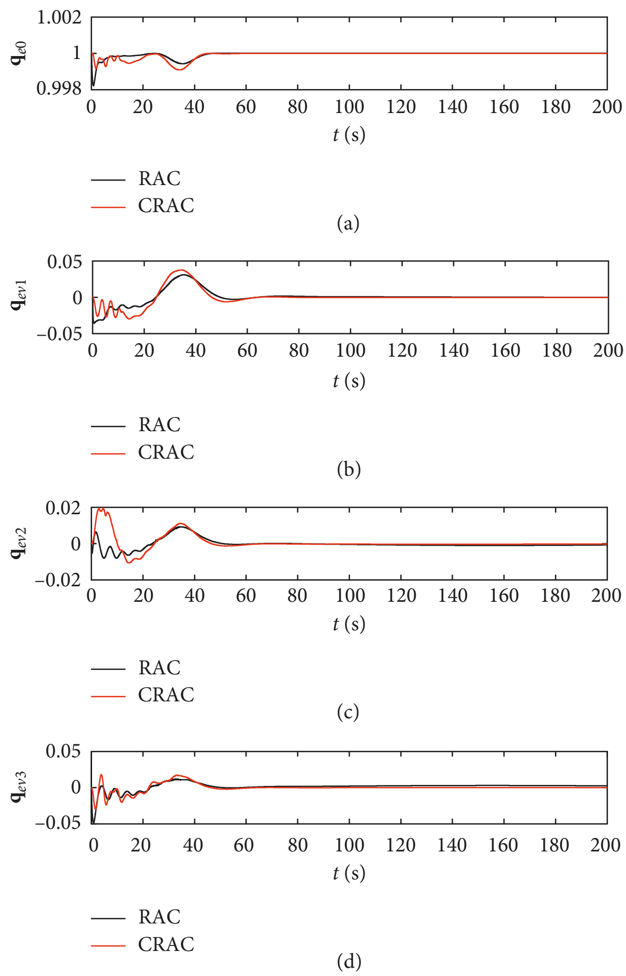

Figure 7: Time response of attitude tracking error in quaternion.

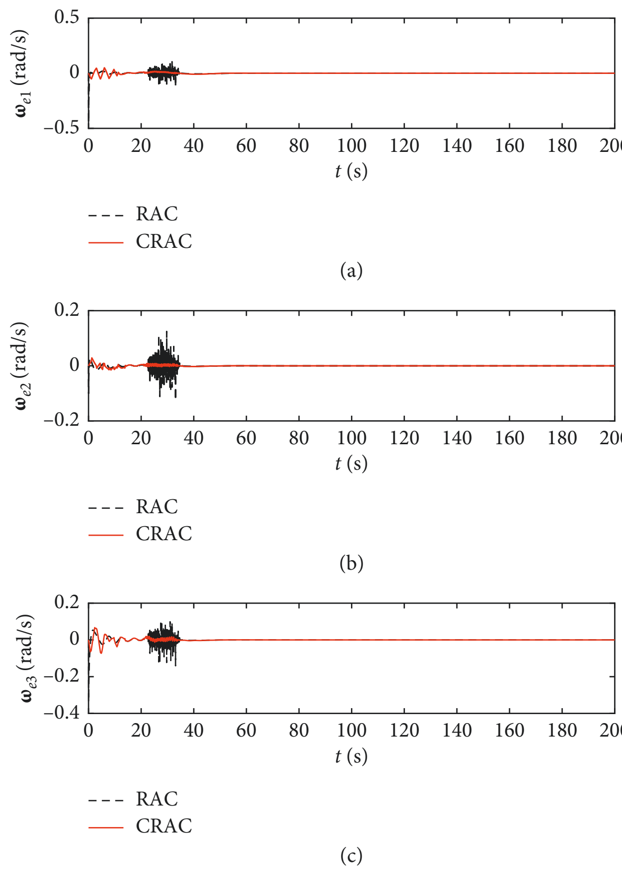

Figure 8: Time response of angular velocity tracking error.

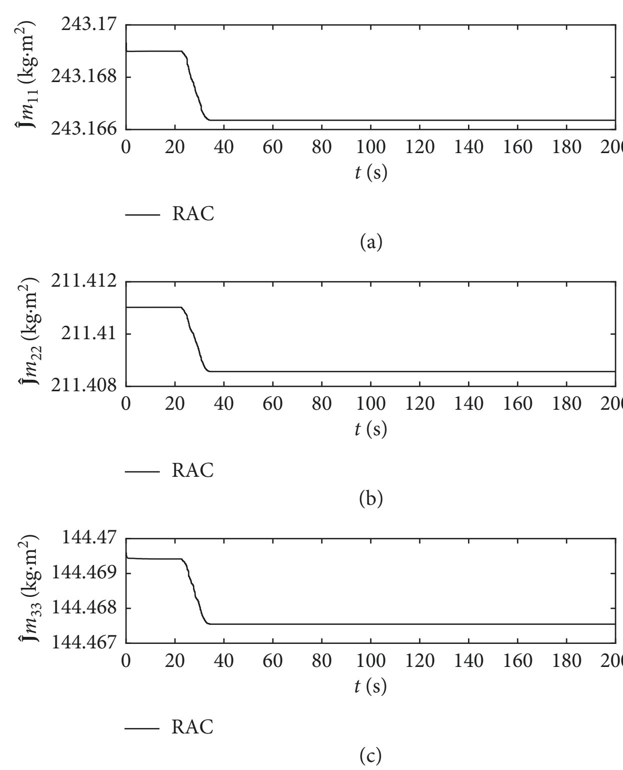

Figure 9: Time response of estimated parameters of inertia in Case 1.

In the following simulations, the control and adaptation gains are provided in Table 2. The maximum output torque of reaction wheel is assumed to be 10 Nm. For the overactuated reaction wheel with configuration misalignments, the normal assembling angles are $\alpha_4 = 35.26$ deg and $\beta_4 = 45$ deg, with the misalignment angles of reaction wheel are, respectively, $\Delta\alpha = [2, 3, 4, 5]^T$deg and $\Delta\beta = [5, 4, 3, 2]^T$deg.

The planned maneuvering path is illustrated in Figures 2–4. For the comparison, the conventional path planning method based on bang-coast-bang (BCB) is also performed at the same simulation conditions. It is illustrated that the maneuver path utilizing planning scheme based on quantic polynomial transition is much smoother than the one by applying conventional method. Smooth angular acceleration variate will introduce the least level of vibration to flexible appendages.

With the application of the proposed CRAC scheme with path planning in Case 2, the simulation results are summarized in Figures 5–21. Since the attitude variables in terms of Euler angles are easier to understand than quaternion, the attitude tracking error in Euler angles denoted as e_φ, e_θ, and e_ϕ are also displayed in Figures 5 and 6.

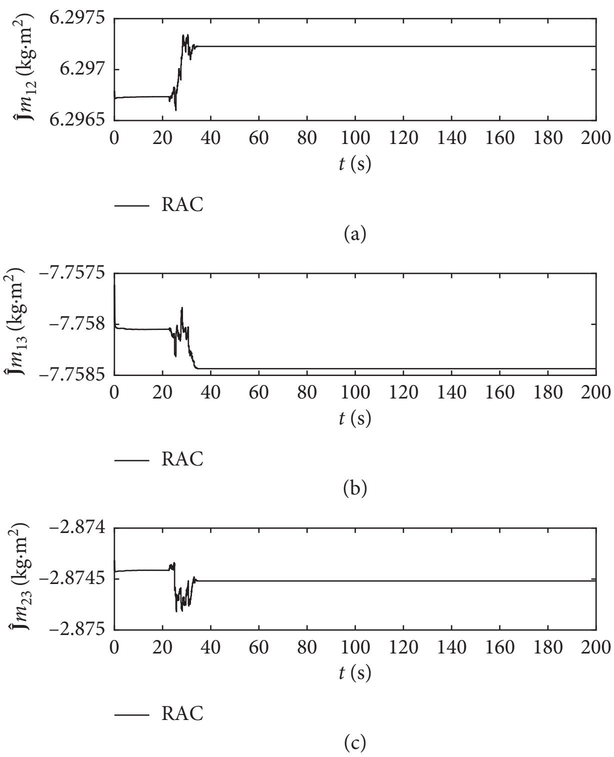

Figure 10: Time response of estimated parameters of the product of inertia in Case 1.

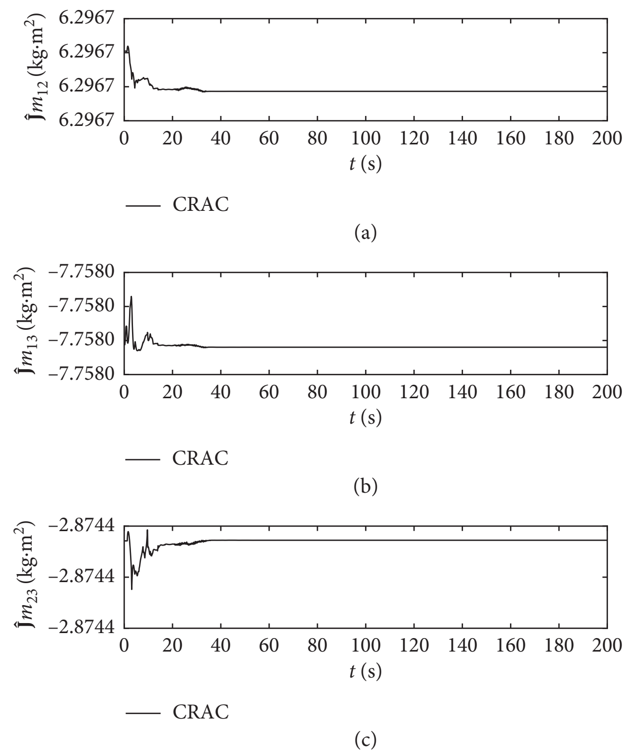

Figure 12: Time response of estimated parameters of the product of inertia in Case 2.

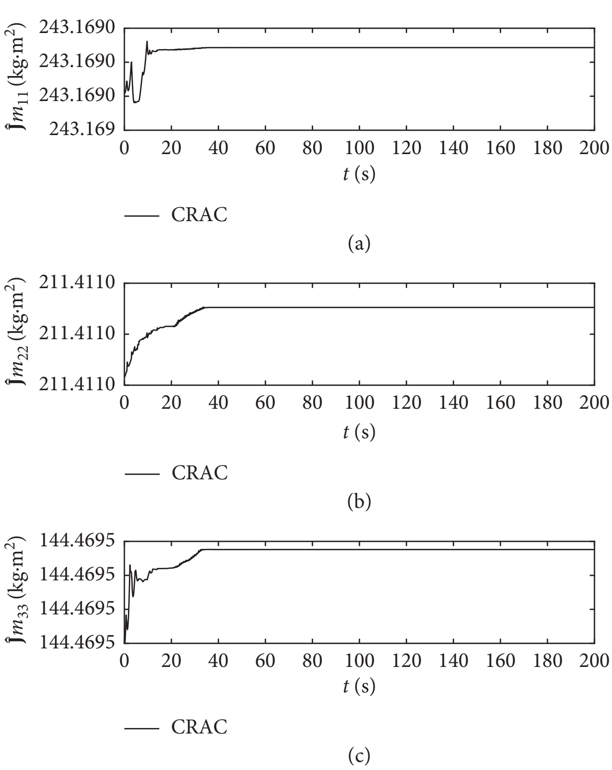

Figure 11: Time response of estimated parameters of inertia in Case 2.

It can been seen from Figures 5, 7, and 8 that it takes about 100 s to drive the tracking errors of attitude Euler angles, attitude quaternion, and angular velocity to their stable points. Through enlarged version of attitude tracking errors illustrated in Figure 6, it can be observed that steady errors of Euler angles are maintained within a range of less than 0.0006 rad. Figure 8 shows the response of angular velocity tracking error, and the steady errors are no more than $2.9e-6$ rad/s. Thus, the high-precision attitude control performance can be achieved despite the presence of parameters uncertainties, external disturbance, actuator saturation, and even actuator misalignments.

The responses of estimated inertial parameters corresponding to update law of (55) and (78) are illustrated in Figures 9–12. It is clear that the convergence of these estimated parameters can be achieved, but not to the true values. That is because sufficient frequency components in the tracking error states are not guaranteed. In other words, the persistent excitation (PE) condition is not satisfied.

The behavior of the modal displacements and their estimates are given in Figure 13. It is noted that all the elastic vibrations and their rates approach zero at time 70 s. It can be observed that not only the vibrations excited by the attitude maneuver are effectively suppressed but also the modal displacements can be well estimated by the modal observer whose performance is explicitly demonstrated in Figure 14. The steady observation errors of modal observer in (37) are tabulated in Table 3.

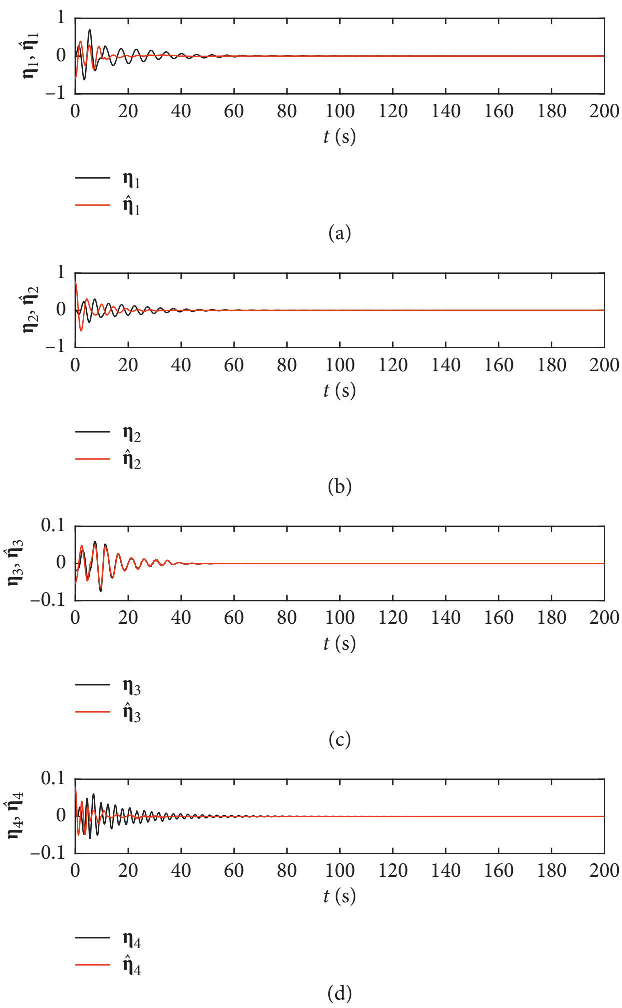

FIGURE 13: Time response of vibration displacements and their estimates.

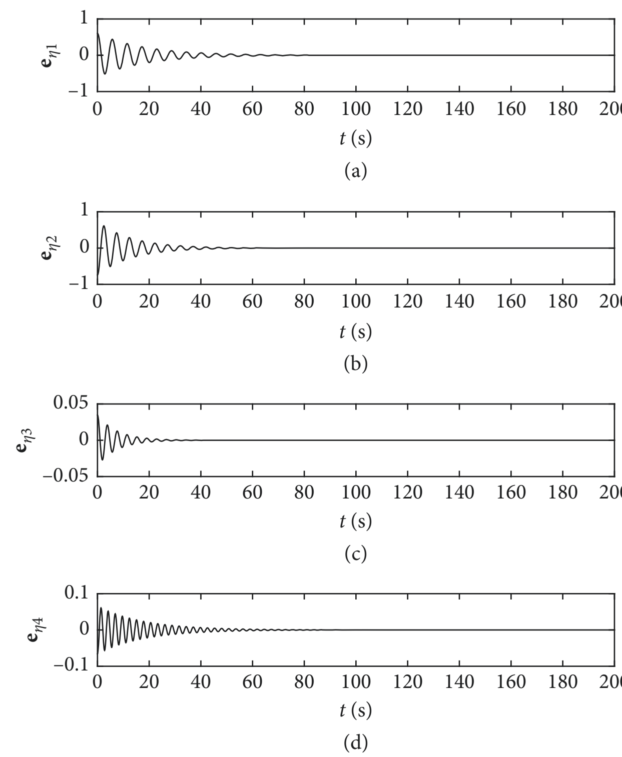

FIGURE 14: Time response of vibration estimate errors.

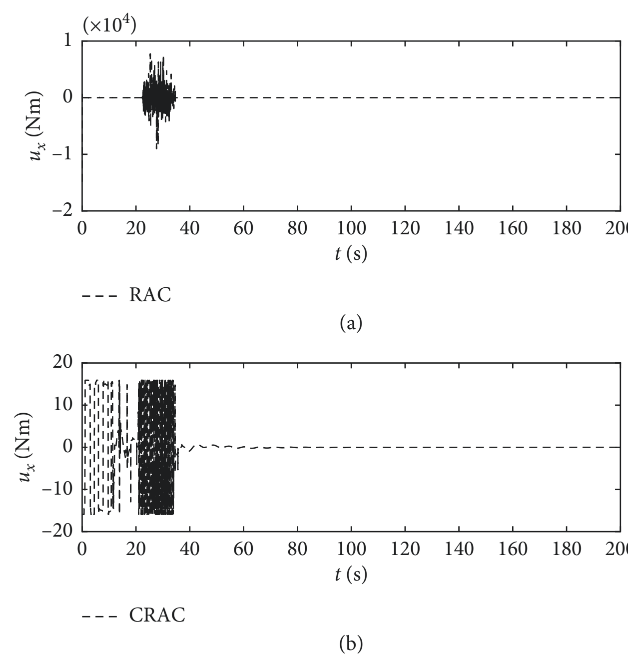

FIGURE 15: Time response of required control torque u_x.

Furthermore, the time responses of total required control torques and reaction wheel output torques are shown in Figures 15–17 and Figures 18–21, respectively. The output torque of each reaction wheel is within the saturation limitation, that is, $\pm$ 10 Nm, which is because the proposed control scheme addresses the control saturation constraints explicitly.

For comparison, the system is also controlled by RAC scheme in Case 1. When it is applied under the same initial conditions and control parameters, the control performance is also illustrated in Figures 5–21 where it is denoted as "RAC."

The steady errors of Euler angles depicted in Figure 6 are 0.005 rad. As demonstrated in Figure 8, it can be observed that severe oscillations of the angular velocity tracking error occur in transient phase and its steady values are no more than $4.1e-5$ rad/s, which are larger than those of the proposed CRAC scheme in Case 2. Thus, although the attitude rotational maneuver using RAC scheme is successfully performed, the control performances are much poorer than those using the proposed CRAC scheme owing to not considering the actuator misalignment.

Further, as is shown in Figures 15–21, the saturation phenomenon of the reaction wheel torques using RAC scheme is not addressed.

Thus, it can be concluded that desired performance of the system can be achieved by the proposed control scheme

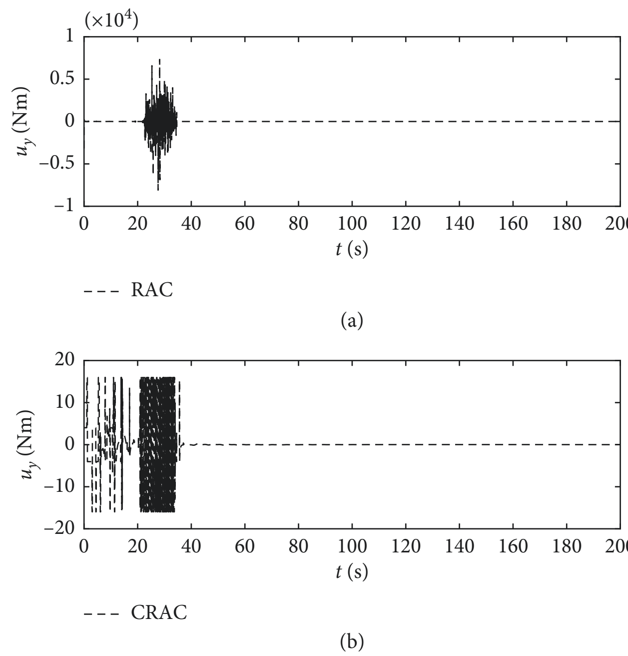

Figure 16: Time response of required control torque u_y.

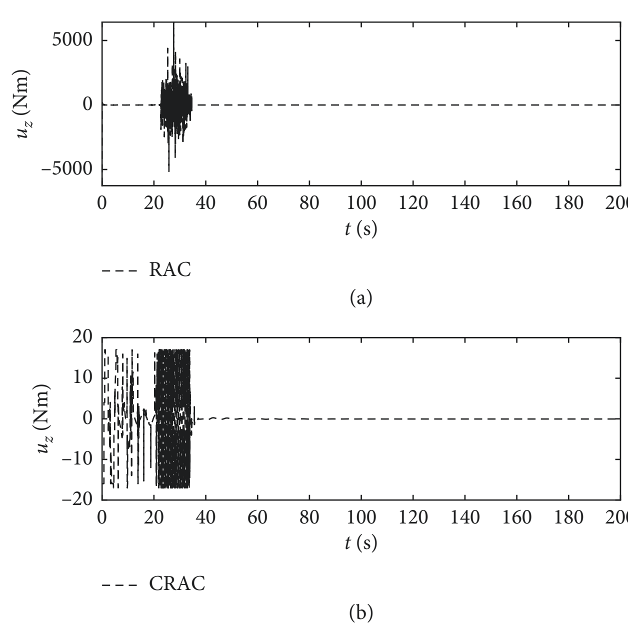

Figure 17: Time response of required control torque u_z.

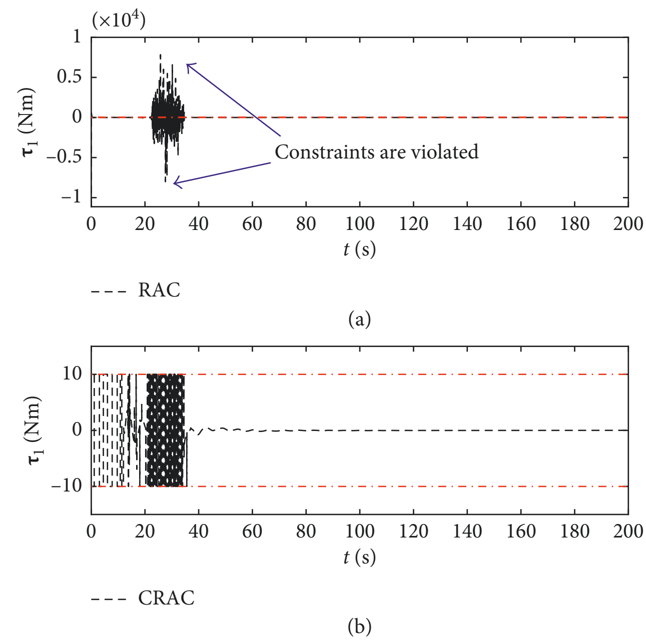

Figure 18: Time response of output torque τ_1.

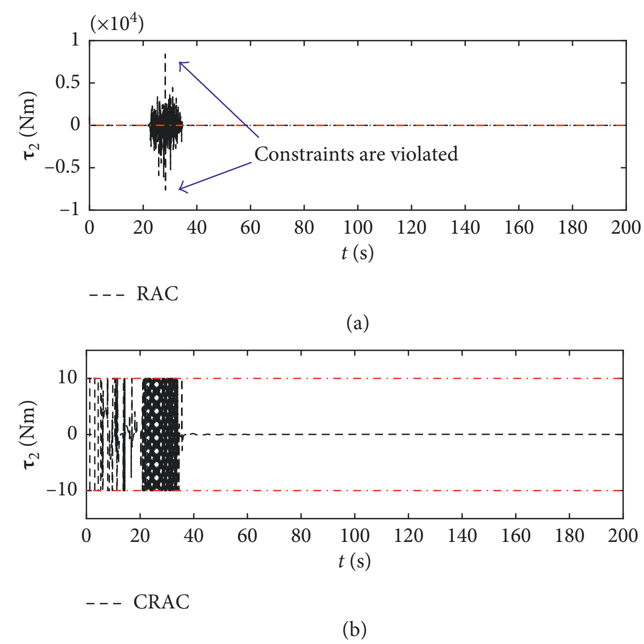

Figure 19: Time response of output control torque τ_2.

subject to multiple undesired constraints including uncertain inertia parameters, external disturbance, unmeasured elastic vibration, actuator saturation, and even actuator misalignment.

5. Conclusion

Taking uncertain inertia parameters, external disturbance, unmeasured elastic vibration, actuator saturation, and even actuator misalignment into account simultaneously, this paper investigates the problem of attitude maneuver and vibration suppression of flexible spacecrafts. Firstly, a new way of path planning, based on quintic polynomial transition, is designed to suppress the flexible appendages' vibration effectively. Then, by utilizing the inherent physical properties of flexible appendages, a modal observer is constructed to supply elastic modal estimates. Plus, an adaptive law is derived so that the requirements to know the prior knowledge of parameter uncertainties and the upper bound of external disturbance is eliminated. In addition, an auxiliary design system is introduced to compensate the actuator saturation effect, and a compensation term is

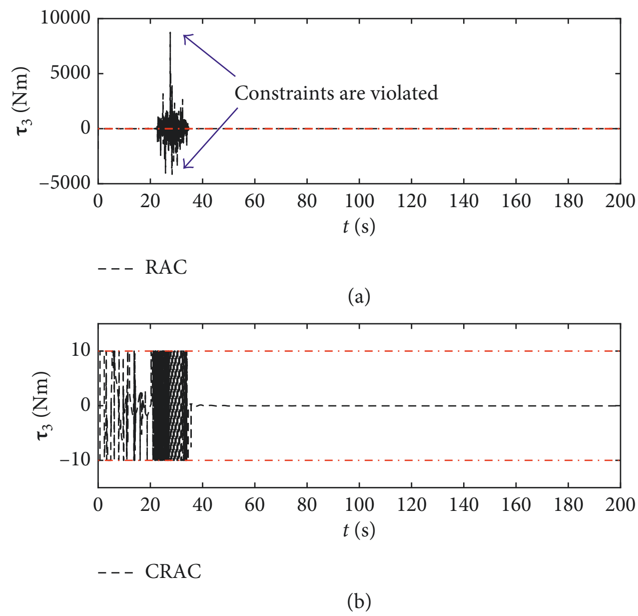

Figure 20: Time response of output control torque τ_3.

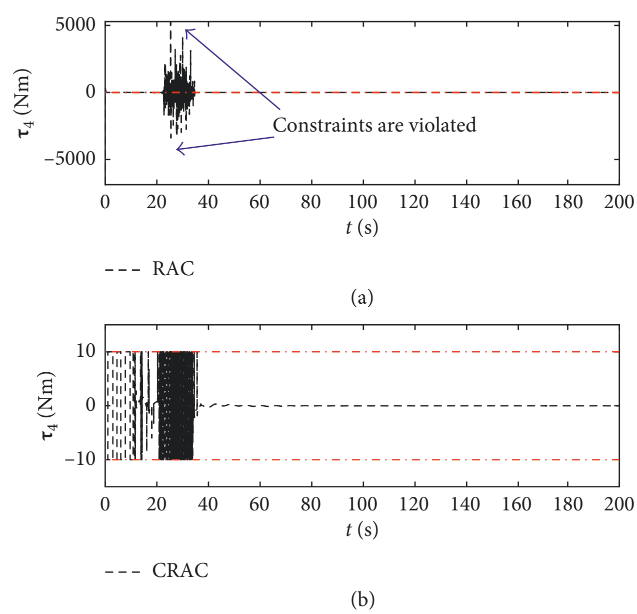

Figure 21: Time response of output control torque τ_4.

Table 3: Steady observation errors of modal observer.

	Steady observation errors
Mode 1 $\lvert\eta_1 - \hat{\eta}_1\rvert$	$7.381e-6$
Mode 2 $\lvert\eta_2 - \hat{\eta}_2\rvert$	$1.61e-7$
Mode 3 $\lvert\eta_3 - \hat{\eta}_3\rvert$	0
Mode 4 $\lvert\eta_4 - \hat{\eta}_4\rvert$	$3.92e-7$

synthesized and integrated into the controller to handle the actuator misalignment. Finally, the stability is rigorously proved and the simulation results demonstrated the effectiveness and robustness of proposed control scheme.

Conflicts of Interest

The authors declare that there are no conflicts of interest regarding the publication of this paper.

References

[1] Y. Guo, C. F. Zhou, Z. Yu, and Q. W. Chen, "Study on attitude control for move-to-rest manoeuvre of flexible spacecraft," *International Journal of Modelling Identification and Control*, vol. 19, no. 1, pp. 23–31, 2013.

[2] Q. Hu and G. Ma, "Vibration suppression of flexible spacecraft during attitude maneuvers," *Journal of Guidance, Control, and Dynamics*, vol. 28, no. 2, pp. 377–380, 2005.

[3] Q. L Hu, P. Shi, and H. J. Gao, "Adaptive variable structure and commanding shaped vibration control of flexible spacecraft," *Journal of Guidance, Control, and Dynamics*, vol. 30, no. 3, pp. 804–815, 2007.

[4] G. B. Maganti and S. N. Singh, "Simplified adaptive control of an orbiting flexible spacecraft," *Acta Astronautica*, vol. 61, no. 7-8, pp. 575–589, 2007.

[5] Q. Hu and G. Ma, "Adaptive variable structure maneuvering control and vibration reduction of three-axis stabilized flexible spacecraft," *European Journal of Control*, vol. 12, no. 6, pp. 654–668, 2006.

[6] C. Pukdeboon and A. Jitpattanakul, "Anti-unwinding attitude control with fixed-time convergence for a flexible spacecraft," *International Journal of Aerospace Engineering*, vol. 2017, Article ID 5018323, 13 pages, 2017.

[7] C. X. Zhong, A. F. Lai, Y. Guo, and Q. W. Chen, "On attitude maneuver control of flexible spacecraft without angular velocity sensors," in *Proceedings of the 2013 IEEE/SICE International Symposium on System Integration*, Kobe, Japan, December 2013.

[8] C. Zhong, Y. Guo, Z. Yu, L. Wang, and Q. Chen, "Finite-time attitude control for flexible spacecraft with unknown bounded disturbance," *Transactions of the Institute of Measurement and Control*, vol. 38, no. 2, pp. 240–249, 2015.

[9] S. D. Gennaro, *Output Attitude Tracking for Flexible Spacecraft*, Pergamon Press, Inc., Oxford, UK, 2002.

[10] S. D. Gennaro, "Output stabilization of flexible spacecraft with active vibration suppression," *IEEE Transactions on Aerospace and Electronic Systems*, vol. 39, no. 3, pp. 747–759, 2003.

[11] S. D. Gennaro, "Passive attitude control of flexible spacecraft from quaternion measurements," *Journal of Optimization Theory and Applications*, vol. 116, no. 1, pp. 41–60, 2003.

[12] S. D. Gennaro, "Tracking control using attitude measurements for flexible spacecraft in presence of disturbances," in *Proceedings of the IEEE Conference on Decision and Control, CDC 2004*, vol. 2, pp. 2123–2128, IEEE, Atlantis, Bahamas, December 2015.

[13] C. Zhong, Z. Chen, and Y. Guo, "Attitude control for flexible spacecraft with disturbance rejection," *IEEE Transactions on Aerospace and Electronic Systems*, vol. 53, no. 1, pp. 101–110, 2017.

[14] J. D. Boskovic, S. M. Li, and R. K. Mehra, "Robust tracking control design for spacecraft under control input saturation," *Journal of Guidance, Control, and Dynamics*, vol. 27, no. 4, pp. 627–633, 2012.

[15] J. D. Boškovic, S. M. Li, and R. K. Mehra, "Robust adaptive variable structure control of spacecraft under control input saturation," *Journal of Guidance, Control, and Dynamics*, vol. 24, no. 1, pp. 14–22, 2001.

[16] C. Pukdeboon, “Inverse optimal attitude stabilization of flexible spacecraft with actuator saturation,” *International Journal of Aerospace Engineering*, vol. 2016, Article ID 1395952, 14 pages, 2016.

[17] Q. Hu and B. Xiao, “Robust adaptive backstepping attitude stabilization and vibration reduction of flexible spacecraft subject to actuator saturation,” *Journal of Vibration and Control*, vol. 17, no. 11, pp. 1657–1671, 2011.

[18] Q. Hu, “Robust adaptive sliding mode attitude maneuvering and vibration damping of three-axis-stabilized flexible spacecraft with actuator saturation limits,” *Nonlinear Dynamics*, vol. 55, no. 4, pp. 301–321, 2009.

[19] A. M. Zou, A. H. J. D. Ruiter, and K. D. Kumar, “Finite-time attitude tracking control for rigid spacecraft with control input constraints,” *IET Control Theory and Applications*, vol. 11, no. 7, pp. 931–940, 2017.

[20] B. Li, Q. Hu, and G. Ma, “Extended state observer based robust attitude control of spacecraft with input saturation,” *Aerospace Science and Technology*, vol. 50, pp. 173–182, 2016.

[21] J. Ma, P. Li, L. Geng et al., “Adaptive finite-time attitude tracking control of an uncertain spacecraft with input saturation,” in *Proceedings of IEEE Conference on Control Applications, CCA 2015*, pp. 930–935, IEEE, Sydney, NSW, Australia, September 2015.

[22] Q. Hu, B. Li, and J. Qi, “Disturbance observer based finite-time attitude control for rigid spacecraft under input saturation,” *Aerospace Science and Technology*, vol. 39, pp. 13–21, 2014.

[23] H. Yoon and P. Tsiotras, “Adaptive spacecraft attitude tracking control with actuator uncertainties,” *Journal of the Astronautical Sciences*, vol. 56, no. 2, pp. 251–268, 2008.

[24] H. C. Lim and H. Bang, “Adaptive control for satellite formation flying under thrust misalignment,” *Acta Astronautica*, vol. 65, no. 1-2, pp. 112–122, 2009.

[25] S. Scarritt, “Nonlinear model reference adaptive control for satellite attitude tracking,” in *Proceedings of AIAA Guidance, Navigation and Control Conference and Exhibit*, p. 7165, Honolulu, HI, USA, August 2008.

[26] M. J. Sidi, *Spacecraft Dynamics and Control*, Cambridge University Press, Cambridge, UK, 1997.

[27] B. Xiao, Q. Hu, and W. Singhose, “Adaptive compensation control for spacecraft attitude stabilization with actuator misalignment and faults,” in *Proceedings of AIAA Guidance, Navigation, and Control Conference*, p. 4626, Minneapolis, MN, USA, August 2012.

[28] X. Huo, Q. Hu, and B. Xiao, “Finite-time attitude control for spacecraft with actuator misalignment,” in *Proceedings of Chinese Control Conference, CCC 2013*, pp. 6197–6201, IEEE, Xi’an, China, July 2013.

[29] A. Zhang, Q. Hu, and X. Huo, “Dynamic control allocation for spacecraft attitude stabilization with actuator uncertainty,” *Proceedings of the Institution of Mechanical Engineers Part G Journal of Aerospace Engineering*, vol. 228, no. 8, pp. 1336–1347, 2014.

[30] M. M. Polycarpou, “Stable adaptive neural control scheme for nonlinear systems,” *IEEE Transactions on Automatic Control*, vol. 41, no. 3, pp. 447–451, 1996.

[31] M. M. Polycarpou and P. A. Ioannou, “A robust adaptive nonlinear control design,” *Automatica*, vol. 32, no. 3, pp. 423–427, 1996.

[32] W. H. Chen, T. Zhang, and M. Q. Cui, “Study of robot trajectory based on quintic polynomial transition,” *Coal Mine Machinery*, vol. 32, no. 12, pp. 49–50, 2011.

[33] Z. Cai, M. S. de Queiroz, and D. M. Dawson, “A sufficiently smooth projection operator,” *IEEE Transactions on Automatic Control*, vol. 51, no. 1, pp. 135–139, 2006.

[34] J. A. Farrell, M. Polycarpou, M. Sharma, and W. Dong, “Command filtered backstepping,” *IEEE Transactions on Automatic Control*, vol. 54, no. 6, pp. 1391–1395, 2009.